Lawrence Berkeley National Laboratory

Title
Chemical Speciation of Sulfur in Marine Cloud Droplets and Particles: Analysis of Individual Particles from Marine Boundary Layer over the California Current

Permalink
https://escholarship.org/uc/item/03231073

Authors
Hopkins, Rebecca J.
William R. Wiley Environmental Sciences Laboratory, Pacific Northwest National Laboratory

Publication Date
2008-03-12

Peer reviewed

1   **Chemical Speciation of Sulfur in Marine Cloud Droplets and Particles:**

2   **Analysis of Individual Particles from the Marine Boundary Layer over**

3   **the California Current.**

4

5   Yuri Desyaterik[†], Rahul A. Zaveri, Carl M. Berkowitz, and Alexander Laskin*
6
7   *William R. Wiley Environmental Molecular Sciences Laboratory and*
8   *Atmospheric Science and Global Change Division,*
9   *Pacific Northwest National Laboratory, Richland, WA 99352, USA*
10
11   Rebecca J. Hopkins[†], Alexei V. Tivanski, Tolek Tyliszczak, and Mary K. Gilles*
12
13   *Chemical Sciences Division and Advanced Light Source*
14   *Lawrence Berkeley National Laboratory, Berkeley, CA 94720-1460, USA*
15
16
17
18
19

20

21

24

25   [†]Authors contributed equally to this work.

26   *Authors to whom correspondence should be addressed:.

27   Alexander Laskin (Alexander.Laskin@pnl.gov)
28   Mary K. Gilles (MKGilles@lbl.gov)
29

30

31   JGR PtReyes_Revised_v6.doc

ABSTRACT

Detailed chemical speciation of the dry residue particles from individual cloud droplets and interstitial aerosol collected during the Marine Stratus Experiment (MASE) was performed using a combination of complementary microanalysis techniques. Techniques include computer controlled scanning electron microscopy with energy dispersed analysis of X-rays (CCSEM/EDX), time-of-flight secondary ionization mass spectrometry (TOF-SIMS), and scanning transmission X-ray microscopy with near edge X-ray absorption fine structure spectroscopy (STXM/NEXAFS). Samples were collected at the ground site located in Point Reyes National Seashore, approximately 1 km from the coast. This manuscript focuses on the analysis of individual particles sampled from air masses that originated over the open ocean and then passed through the area of the California current located along the northern California coast. Based on composition, morphology, and chemical bonding information, two externally mixed, distinct classes of sulfur containing particles were identified: chemically modified (aged) sea salt particles and secondary formed sulfate particles. The results indicate substantial heterogeneous replacement of chloride by methanesulfonate ($CH_3SO_3^-$) and non-sea salt sulfate (nss-SO_4^{2-}) in sea-salt particles with characteristic ratios of nss-S/Na > 0.10 and $CH_3SO_3^-$/nss-SO_4^{2-} > 0.6.

1. INTRODUCTION

Aerosols in the unpolluted marine boundary layer (MBL) result from two major sources. First, sea salt particles generated from wave action, which are typically micrometers or larger in size. Second, acidic sulfate aerosol formed by nucleation, with sizes on the order of tenths of a micrometer. This mixture of particle types evolves with time due to a number of processes, including deposition of condensable species, uptake of gas-phase species and a variety of heterogeneous gas-to-particle and homogenous in-particle chemical reactions. Increased interest in the chemical composition and heterogeneity of marine aerosols stems from their regional and global impact on sulfur oxidation in the MBL, in addition to climate effects arising from light scattering and cloud condensation nuclei (CCN) activity [*Covert, et al.*, 1992; *Gong*, 2003; *Gong and Barrie*, 2003; *Gong, et al.*, 1997; *Gong, et al.*, 2002; *Lewis and Schwartz*, 2004; *Murphy, et al.*, 1998; *Quinn, et al.*, 1993; *Sievering, et al.*, 1991; *Sievering, et al.*, 2004].

The major gaseous precursor for marine sulfur-containing aerosol is dimethyl sulfide (DMS). DMS is produced and emitted into the atmosphere by marine phytoplankton [*Keller, et al.*, 1989]. Current estimates of global emissions indicate that DMS is the largest source of natural sulfur [*Bates, et al.*, 1992; *Kettle, et al.*, 1999], produced at a rate of $\sim$12 Tg S yr^{-1} [*Spiro, et al.*, 1992]. In the atmosphere, DMS undergoes a complex sequence of gas-phase oxidation reactions, producing a wide variety of oxidized products, which in turn interact with marine cloud droplets and aerosols. These interactions include nucleation of new particles and the alteration of pre-existing droplets and aerosols through condensation and multiphase chemistry. Due to its large flux, the atmospheric cycle of DMS significantly impacts the radiative budget over oceans on regional and global scales [*Charlson, et al.*, 1987; *Shaw*, 1983].

3

73   The atmospheric chemistry of DMS and its possible impact on aerosols and cloud

74   droplets is the subject of many studies. Understanding its major reactions has been achieved

75   through computer kinetic modeling studies [*Charlson, et al.*, 1987; *Kerminen, et al.*, 1998; *Koga*

76   *and Tanaka*, 1993; 1996; 1999; *Koga, et al.*, 1991; *Lucas and Prinn*, 2002; 2003; 2005a; b; *Shaw*,

77   1983; *von Glasow and Crutzen*, 2004; *von Glasow, et al.*, 2002a; b; *Yin, Grosjean, Flagan, et al.*, 1990;

78   *Yin, et al.*, 1986; *Yin, Grosjean and Seinfeld*, 1990; *Zaveri*, 1997], focused laboratory studies

79   [*Arsene, et al.*, 2002; *Barnes, et al.*, 1994; *Barone, et al.*, 1996; *Hynes, et al.*, 1995; *Hynes and Wine*,

80   1996; *Hynes, et al.*, 1986; *Ravishankara, et al.,* 1997; *Stickel, et al.*, 1992; *Turnipseed, et al.,* 1997;

81   *Urbanski, et al.*, 1998; *Yin, et al.*, 1986; *Zhao, et al.*, 1996; *Zhu, et al.*, 2006; *Zhu, et al.*, 2003], and

82   field observations [*M. O. Andreae and Raemdonck*, 1983; *T. W. Andreae, et al.*, 1993; *Bandy, et al.*,

83   1992; *Bandy, et al.*, 2002; *Barnard, et al.*, 1982; *Cooper and Saltzman*, 1991; 1993; *Spicer, et al.*,

84   1996; *Zemmelink, et al.*, 2002]. A simplified schematic diagram illustrating DMS chemistry and

85   its climate links is presented in Figure 1. In the ambient atmosphere, oxidation of DMS is

86   initiated by reaction with a variety of atmospheric free radicals. These radicals include, but

87   are not limited to, OH, NO_3, $O(^3P)$, Cl, Br, and BrO. Such reactions proceed *via* two

88   generalized reaction pathways: either addition of an O atom and/or abstraction of an H

89   atom. The branching ratio between the two generalized pathways is temperature dependent

90   with H abstraction dominating at room temperature, while O addition becomes increasingly

91   important at temperatures below 280 K [*Hynes, et al.*, 1986; *von Glasow and Crutzen*, 2004].

92   DMS gas phase oxidation products include sulfur dioxide (SO_2), sulfuric acid (H_2SO_4),

93   dimethylsulfoxide (CH_3SOCH_3), methanesulfinic acid ($CH_3S(O)OH$), methanesulfonic acid

94   (CH_3SO_3H, MSA), in addition to other species [*Lucas and Prinn*, 2002; *von Glasow and Crutzen*,

95   2004; *Yin, Grosjean, Flagan, et al.*, 1990; *Zaveri*, 1997].

96　　　　Under atmospheric conditions, H_2SO_4 is the only DMS oxidation product that forms

97　　new non-sea salt sulfate (nss-SO_4^{2-}) particles (new CCN) that could potentially increase the

98　　cloud albedo. All other products condense onto pre-existing particles, primarily sea salt,

99　　leading to changes in particle composition and particle size without formation of new CCN.

100　Fewer and larger particles of mixed sea salt/$CH_3SO_3^-$/nss-SO_4^{2-} composition would reduce

101　cloud albedo and increase the wash-out of particles due to collision coalescence, therefore

102　reducing cloud lifetime. Hence, the partitioning between DMS oxidation products in

103　different atmospheric environments may affect the number and size of CCN, which impacts

104　the chemistry-cloud-climate feedback in the marine atmosphere. For the remainder of this

105　work, methanesulfonate and sulfate are referred to as the anions $CH_3SO_3^-$ and SO_4^{2-}

106　respectively, as in our samples they are present in crystalline form. Their cation pairing may

107　include an array of ions typical for sea salt, i.e. Na^+, Mg^{2+}, K^+ and others that are omitted for

108　clarity.

109　　　　For a specific set of atmospheric conditions, consecutive uptake of the DMS

110　oxidation products onto cloud droplets and their subsequent oxidation in the aqueous phase,

111　results in different partitioning between $CH_3SO_3^-$ and nss-SO_4^{2-}. Kinetic modeling studies of

112　the $CH_3SO_3^-$/nss-SO_4^{2-} partitioning in marine aerosol predict formation of minor amounts

113　of $CH_3SO_3^-$ and favor production of nss-SO_4^{2-} in sea salt particles under a variety of

114　atmospheric conditions [*Hertel, et al.*, 1994; *Kerminen, et al.*, 1998; *Kloster, et al.*, 2006; *Koga and*

115　*Tanaka*, 1996; 1999; *Lucas and Prinn*, 2002; *Yin, Grosjean, Flagan, et al.*, 1990; *Zaveri*, 1997].

116　Measured values of $CH_3SO_3^-$/nss-SO_4^{2-} ratios in bulk samples typically span a range from

117　0.001 (low latitudes) to 0.6 (high latitudes) [*Allen, et al.*, 1997; *Berresheim, et al.*, 1990;

118　*Burgermeister and Georgii*, 1991; *Galloway, et al.*, 1993; *Ganor, et al.*, 2000; *Kouvarakis and*

119　*Mihalopoulos*, 2002; *Li and Barrie*, 1993; *Li, Barrie and Sirois*, 1993; *Li, Barrie, Talbot, et al.*, 1993;

120   *Li, et al.*, 1996; *Mihalopoulos, et al.*, 1992; *Saltzman, et al.*, 1985; 1986; *Saltzman, et al.*, 1983;

121   *Sciare, et al.*, 2000; *Wylie and deMora*, 1996]. Recent modeling studies indicate that under

122   certain conditions $CH_3SO_3^-$/nss-SO_4^{2-} ratios as high as $1.2 - 3.3$ in marine droplets can occur

123   [*von Glasow and Crutzen*, 2004]. Specifically, high $CH_3SO_3^-$/nss-SO_4^{2-} values resulted from

124   model simulations for the cloudy MBL in winter conditions (surface temperature of 3-8°C

125   over the ocean). The authors concluded that these high ratios could result from previously

126   overlooked halogen chemistry that favors production of $CH_3SO_3^-$ under cold cloud

127   scenarios.

128   The high level of detail used in this model was in principle sufficient to distinguish

129   and predict $CH_3SO_3^-$/nss-SO_4^{2-} ratios in droplets and particles of different origin, *i.e.* sea salt

130   *versus* sulfate particles [*von Glasow and Crutzen*, 2004]. However, validation of these

131   calculations requires field or laboratory data with a similar level of specificity. In this

132   manuscript we report results from single particle analysis of dry residues of cloud droplets

133   and interstitial aerosol that provide information on $CH_3SO_3^-$/nss-SO_4^{2-} ratios in individual

134   marine particles for the first time.

135   Samples were collected during the Marine Stratus Experiment (MASE) of July 2005

136   at the Point Reyes National Seashore located north of San Francisco [*MASE*, 2005]

137   (*http://www.asp.bnl.gov/MASE.html*). This field study provided an excellent opportunity to

138   sample marine particles under relatively cold cloudy conditions, which according to the

139   modeling predictions of *von Glasow and Crutzen* [*von Glasow and Crutzen*, 2004], could display

140   elevated $CH_3SO_3^-$/nss-SO_4^{2-} ratios. At the northern coast of California, cold ocean currents

141   produce preferential upwelling, resulting in low ocean temperatures (~10-15° C) even during

142   summer time. In addition, low altitude clouds form and typically shroud this region during

143   the summer months. This region is also an area of phytoplankton bloom, resulting in

144   efficient DMS production [*Strub, et al.*, 1990; *A. Thomas and Strub*, 2001; *A. C. Thomas and*

145   *Strub*, 1990]. These factors provide a unique opportunity for field studies of $CH_3SO_3^-$ and

146   nss-SO_4^{2-} partitioning in marine cloud droplets and particles representative of relatively cold

147   marine atmosphere over an area rich in DMS.

148   The complementary capabilities of three analytical techniques provide complete

149   chemical speciation of the field collected marine particles, with the aim of identifying the

150   chemical forms of particulate sulfur. The three data sets are consistent with one another and

151   indicate enhanced formation of particulate $CH_3SO_3^-$ in sea salt droplets and particles

152   collected during MASE. This unique combination of single-particle measurements enables

153   quantitative assessment of $CH_3SO_3^-/nss-SO_4^{2-}$ ratios in individual particles.

154

155   **2.   EXPERIMENTAL**

156   2.1.   **Meteorological Conditions and Sample Collection.** Particle samples were

157   collected continuously during the cloudy period between July 6th 17:00 –July 7th 9:00 Pacific

158   Standard time (July 7th 01:00 – 17:00, UTC) on a seashore site within one kilometer of the

159   Pacific Ocean at the Point Reyes National Seashore, N38°5´, W122°57.43´. This site is

160   shrouded in cold clouds much of the time, as illustrated in Figure 2, and is well situated for

161   sampling cloud droplets and aerosols. Figure 2 shows backward trajectory calculations

162   performed using the HYSLPIT model [*Draxler and Rolph*, 2003], that end at the sampling site

163   on July 6, 21:00 PST (red) and July 7, 09:00 PST (blue). The trajectories indicate that during

164   the 36 hours preceding collection, the air mass passed over open areas of the ocean and then

165   along the northern shore of California. Backward trajectories calculated for 5 days prior to

166   collection revealed that the sampled air traveled over the Pacific Ocean and did not enter

167   continental areas in exception to ~1-2 km of the shore area adjacent to the sampling site.

168 Over the time frame of the backward trajectory calculation shown in Figure 2b, the relative

169 humidity was above 78%, the air temperature was 13-16°C and the height of boundary

170 mixing layer was 250-400 meters.

171 During sampling, the cloud/fog droplets and (interstitial) aerosol were first separated

172 using a counter-flow virtual impactor (CVI) [*Ogren, et al.*, 1985] that directs the flow of small

173 (interstitial) particles and relatively large cloud droplets into two different sampling lines: the

174 CVI line for particles (drops) larger than ~5 µm and the aerosol observing system (AOS)

175 line for particles smaller than ~5 µm. The particles were first dried inside the CVI and AOS

176 probe lines, and the resulting dehydrated particles were collected by two compact time

177 resolved aerosol collectors (TRAC) [*Laskin, et al.*, 2006; *Laskin, Iedema, et al.*, 2003] attached

178 to each of the lines. The TRAC is a conventional one stage jet-to-plate impactor that

179 deposits particles on a rotating impaction plate containing pre-arranged substrates. In this

180 study, each substrate was exposed for 12 minutes of sample collection. The effective

181 aerodynamic cut-off size D_{50} of the TRAC is ~0.36 µm. Three different types of substrates

182 were used in this study: (a) Copper 400 mesh TEM grids coated with Carbon Type-B films

183 (Ted Pella, Inc.) for the CCSEM/EDX analysis, (b) silicon wafer chips (Silson Ltd, Inc.) for

184 the TOF-SIMS analysis, and (c) silicon wafer frames with silicon nitride windows (Silson

185 Ltd, Inc.) for the STXM/NEXAFS analysis. After collection, impaction plates with the

186 exposed substrates were sealed and stored pending analysis.

187 In general, particle samples collected on substrates may suffer from some artifacts.

188 These include evaporation of volatile and semi-volatile species during the sampling, storage

189 and then analysis by the applied techniques as well as possible reactions between sampled

190 particles and trace gases entering the impactor. For $CH_3SO_3^-$ and SO_4^{2-} salts, no sampling

191 artifacts due to the volatilization are expected to occur. Artifacts like the potential reactions

192 of $SO_2(g)$, $HCl(g)$ and $NO_2(g)$ with the samples inside the TRAC, could not be quantified.

193 However, their possible impacts were somewhat minimized by drying particles prior to

194 collection which would decrease their reaction kinetics.

195 **2.2. Methods of laboratory analysis.** Detailed characterization of individual

196 particles required multiple techniques. As illustrated below, applications of different

197 analytical methods are interdependent; hence, the information from one method guides

198 subsequent measurements. Three analytical techniques were applied for particle analysis: (a)

199 CCSEM/EDX – for microscopy imaging of particles and quantitative speciation of their

200 elemental composition, (b) TOF-SIMS – for qualitative detection of $CH_3SO_3^-$ and SO_4^{2-}

201 within individual particles, and (c) STXM/NEXAFS – for quantitative speciation of the

202 $CH_3SO_3^-$ to SO_4^{2-} partitioning within individual particles.

203 A FEI XL30 digital field emission gun environmental scanning electron microscope

204 was used in this work. The microscope is equipped with an EDAX PV7761/54 ME X-ray

205 spectrometer (EDAX, Inc) with a Si(Li) detector with an active area of 30 mm^2 and an

206 ATW2 window. In addition to the standard SEM/EDX mode of operation, the instrument

207 can also operate in computer-controlled (CCSEM/EDX) mode for analysis of individual

208 particles. In the CCSEM/EDX mode, selected samples are inspected automatically and

209 individual particles are recognized by an increase in the detector signal above a threshold

210 level. The program then acquires an X-ray spectrum from each detected particle. In this

211 work, particles with an equivalent circle diameter larger than ≥ 0.35 μm were measured by

212 the software. The X-ray spectra were acquired for 10 s, at a beam current of ~500 pA and an

213 accelerating voltage of 20 kV. Additional details of the CCSEM/EDX approach employed

214 for the analysis of particles deposited onto carbon coated TEM grids can be found in our

215 recent review article [*Laskin, et al.*, 2006] and references therein.

216   A TRIFT II time-of-flight secondary ion mass spectrometer (TOF-SIMS), (Physical

217   Electronics, Inc.) was used in this work. TOF-SIMS analysis entails impacting a pulsed

218   primary ion beam onto a solid sample in vacuum and collecting secondary ions of one

219   polarity (positive or negative), using a time-of-flight (TOF) mass analyzer. The particles

220   collected on the silicon wafer chips were placed in the sample holder and subject to a $^{69}Ga^+$

221   source of primary ions in high spatial resolution mode. An accelerating voltage of 15 kV was

222   used for spectral measurements and 25 kV for mapping. The dose rate was 9.8×10^{12} ions

223   cm^{-2}. A combination of static and dynamic modes of operation allowed molecular speciation

224   of different forms of sulfur-containing compounds within individual particles.

225   STXM/NEXAFS measurements were performed at the carbon (C) (280 – 320 eV)

226   and nitrogen (N) (395 – 430 eV) K-absorption edges and at the sulfur (S) (168 – 176 eV) L-

227   absorption edge. STXM instruments at beamlines 5.3.2 (C, N) and 11.0.2. (C, N, S) of the

228   Advanced Light Source of Lawrence Berkeley National Laboratory were used for these

229   experiments. The intensity of X-rays transmitted through the sample at a fixed energy is

230   measured as the sample is raster scanned to record an image. Sequences of images are

231   acquired at closely spaced energies to record a "stack" of images, which is essentially a three-

232   dimensional map in position, energy and transmission. NEXAFS spectra from individual

233   pixels or particular regions of interest on the sample image are extracted from the stack. The

234   absorption through the sample is obtained by converting the signal (Beer-Lambert Law)

235   using the reference flux measured through a sample free region. This mapping of chemical

236   bonding information in individual particles [*Hopkins, Tivanski, Marten, et al.*, 2007; *Tivanski, et*

237   *al.*, 2007; *Maria, et al.*, 2004; *Russell, et al.*, 2002] allows a quantitative assessment of the

238   apportionment between different molecular forms of the same element, *i.e.* $CH_3SO_3^-$ and

239   SO_4^{2-} in this work. For comparison purposes, particles of reference materials were examined

240 using TOF-SIMS and STXM/NEXAFS, including sodium sulfate (Na_2SO_4) (99.99% pure),

241 sodium methanesulfonate (CH_3SO_3Na) (98% pure) and ammonium sulfate ((NH_4)$_2SO_4$)

242 (99.99% pure) purchased from Sigma-Aldrich.

243

244 **3. EXPERIMENTAL RESULTS AND DISCUSSIONS**

245 Twelve samples (6 CVI and 6 AOS samples with time intervals of ~1.5-2 hours

246 between them) from the Point Reyes sampling site collected during the cloudy period were

247 analyzed using CCSEM/EDX single particle analysis. Figure 3 shows typical SEM images of

248 CVI and AOS aerosol samples. The upper images depict samples collected on silicon wafer

249 chips, while the magnified bottom images are from samples collected on TEM grid

250 supported films. As seen from the upper images, the spatial distribution of particles is

251 inhomogeneous. Larger particles are concentrated in the central region, directly under the

252 deposition nozzle and smaller particles are scattered widely from this area. Thus, a

253 statistically significant analysis of particles by CCSEM/EDX requires sampling across the

254 deposition spot, as indicated by the rectangles in the images. The elemental composition was

255 analyzed for ~1000 particles in a region of 500 μm × 80 μm across the deposition spot for

256 each tested sample.

257 A brief inspection using manual SEM/EDX analysis indicated two prominent

258 particle classes, characteristic for both the CVI and AOS samples. The particles were mostly

259 either sea salt or sulfur-rich (S-rich) particles. S-rich particles are composed of a mixture of

260 H_2SO_4 and (NH_4)$_2SO_4$, as discussed below. Sea salt particles are easily recognized (Figure 3,

261 bottom panels) as they are typically of super micron size with cubic-shaped NaCl crystals

262 surrounded by irregularly shaped residues of other salts. In contrast, S-rich particles are

263 submicron in size and spherical. Consistent with the schematic of sulfur-aerosol-climate links

264 presented in Figure 1, larger sea salt particles dominate the CVI samples while smaller S-rich

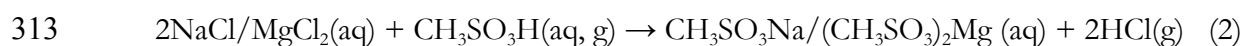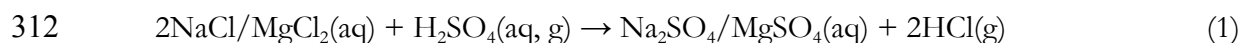265 particles are more abundant in the AOS samples.

266 In this work, as illustrated in panel (a) of Figure 4, a simple rule-based assignment

267 was used to separate individual particles into three major classes. All particles (~10,000)

268 detected in the CCSEM/EDX analysis of 12 selected samples are combined in a group and

269 then all particles containing sulfur above the threshold level of 0.5 atomic percent (as

270 detected by the EDX analysis) are separated. Next, sulfur containing particles that also

271 contain sodium are assigned into the "sea salt" class, while those containing only S, O, and

272 N are assigned to the "S-rich" class. Particles in the S-rich class are expected to display

273 mixed H_2SO_4 and $(NH_4)_2SO_4$ composition. All remaining particles are assigned to one, non-

274 specific class of "other" particles. Panel (b) of Figure 4 illustrates the results of this

275 classification scheme for particles sampled from the CVI and AOS lines over the cloudy

276 period studied here. In general, significant populations of sea salt particles dominate samples

277 collected from both sampling lines, indicating that even submicron particles typical for the

278 AOS samples are of sea mist origin rather than sulfates formed by nucleation. Nucleated

279 sulfates presumably fall into the "S-rich" class and their relative population ranges from

280 between $2-6\%$ and $15-30\%$ in the CVI and AOS samples, respectively. Relative

281 contributions of "other" particles normally remains at the $3-5\%$ level and only occasionally

282 reaches values of $8-9\%$. Particle class composition remained largely the same over the

283 entire period of the cloudy episode for both sampling lines.

284 Figure 5 illustrates particle number size distributions of sea salt and S-rich particles

285 determined from the CCSEM/EDX data, combined for the 6 CVI and 6 AOS analyzed

286   samples. The four distributions are normalized to the total number of particles. Plots

287   presented in panels (a) and (b) are shown on the same scale to facilitate comparison. Hence,

288   areas below the distribution curves indicate relative populations of each particle class. The

289   size distributions in Figure 5 indicate a mode size of ~0.8 μm for residues of sea salt

290   particles in the CVI samples. A smaller mode size of 0.4-0.5 μm is observed for sea salt

291   particles in the AOS samples. The number concentration ratio of sea salt particles found in

292   the CVI samples to those in the AOS samples is approximately 2:1. The situation is reversed

293   for the S-rich particles where the concentration of S-rich particles in the AOS sample is ~2

294   times higher than for the CVI samples. The size distributions of S-rich particles peak at ~0.5

295   μm and ~0.4 μm for the CVI and AOS samples, respectively. However, the abrupt fall-off of

296   the size distributions at ~0.3-0.4 μm is due to the impactor cut-off function and

297   comparisons of the size distributions in Figure 5 must be made with this caveat in mind.

298   The CCSEM/EDX analysis indicates sulfur enrichment in sea salt particles. Figure 6

299   shows the CCSEM/EDX measured S/Na elemental ratios for sea salt particles detected in

300   the CVI (upper panel) and AOS (bottom panel) samples. The dashed horizontal line is the

301   nominal ratio of S/Na = 0.06, typical for sea water [*CRC*, 1999]. The solid curved line

302   indicates the experimentally determined deviation of the S/Na ratios for large sea salt

303   particles. This deviation is a result of ZAF sensitivity effects [*Goldstein, et al.*, 2003], which

304   were omitted from the quantification method [*Laskin and Cowin*, 2001; *Laskin, et al.*, 2006].

305   The S/Na elemental ratios are systematically higher than expected for unreacted sea salt

306   particles. This indicates cloud and chemical processing of sea salt particles with sulfur

307   compounds, which is consistent with the DMS chemistry expected in the region of this field

308   campaign.

309   For cloud and chemically processed sea salt particles, chemical reactions of sea salt

310   components and added sulfuric and/or methanesulfonic acids can be presented by the

311   following, highly simplified, albeit illustrative reactions:

312      $2NaCl/MgCl_2(aq) + H_2SO_4(aq, g) \rightarrow Na_2SO_4/MgSO_4(aq) + 2HCl(g)$ (1)

313      $2NaCl/MgCl_2(aq) + CH_3SO_3H(aq, g) \rightarrow CH_3SO_3Na/(CH_3SO_3)_2Mg (aq) + 2HCl(g)$ (2)

314 These reactions liberate HCl gas to the atmosphere, leaving particles enriched in sulfur and

315 depleted in chloride. Additional sulfur-halogen processes could also lead to similar changes

316 in the elemental composition of sea salt particles [*Finlayson-Pitts*, 2003; *Finlayson-Pitts and*

317 *Hemminger*, 2000]. However, a full discussion of the detailed reaction mechanism and its

318 kinetics is beyond the scope of this manuscript.

319   The sulfur enrichment is larger for sea salt particles in the CVI samples, compared to

320 those in the AOS samples. This is likely a result of the greater activation of particles (larger

321 droplets and higher water content) sampled in the CVI line, compared to the smaller sizes

322 sampled in the AOS line. If so, the higher water content would provide an enhanced

323 capacity for soluble species in larger droplets, and therefore higher S/Na ratios in the CVI

324 samples of dry residues would be expected.

325   CCSEM/EDX analysis provides quantitative data on the S/Na ratios over a

326 statistically significant number of particles. However, no molecular information on the

327 chemical forms of sulfur can be inferred from EDX spectroscopy. Molecular speciation of

328 sulfur-containing compounds is revealed by complementary analysis of individual particles

329 using TOF-SIMS. To identify chemical forms of sulfur, TOF-SIMS ionic maps were

330 produced for selected ions indicative of sulfate (SO_4^-, HSO_4^-), methanesulfonate (SO_3^-,

331 $CH_3SO_3^-$), sodium (Na^+) and ammonium (NH_4^+). Figure 7 shows ionic maps (100 μm × 100

14

332 μm) characteristic for CVI samples collected during this cloudy period. The maps indicate

333 that methanesulfonate (SO_3^-, $CH_3SO_3^-$) ions are co-located with Na^+ ions, while sulfate

334 (SO_4^{2-}, HSO_4^-) ions are co-located with NH_4^+ ions. Furthermore, the characteristic locations

335 of sulfate and the methanesulfonate ions do not overlap. These observations support the

336 conclusion that methanesulfonate is present in relatively large sea salt particles, while the

337 characteristic sulfate ions are primarily generated from smaller $(NH_4)_2SO_4$ particles. To

338 confirm this conclusion, TOF-SIMS negative spectra integrated from the areas of sea salt

339 and $(NH_4)_2SO_4$ particles were compared with those acquired from laboratory prepared

340 samples of CH_3SO_3Na and $(NH_4)_2SO_4$ particles. This comparison is shown in Figure 8. The

341 characteristic spectra of field collected particles match those of the standard materials nearly

342 perfectly. Although not shown here, negative spectra of Na_2SO_4, CH_3SO_4Na, and HO-

343 CH_2SO_3Na particles were also measured (see supplement A), and did not match the spectra

344 measured in the field samples.

345 However, these TOF-SIMS observations should be interpreted with some caution.

346 Particles were examined with a low primary ion dose (static mode of operation), resulting in

347 an analysis depth of 3 – 5 nm, thus corresponding to the outermost atomic layers of the

348 particles. As particles dry out, the less soluble salts precipitate first and form the core of the

349 particle, while more soluble salts are present in the outer layer. Thus, the observed abundant

350 mass spectrometry signal originating from the highly soluble CH_3SO_3Na salt does not

351 confirm the absence of sulfates in these sea salt particles as sulfates could be present at the

352 particle core, and therefore not detectable in this operating mode of the TOF-SIMS

353 instrument. Nevertheless, the important observation is that the $(NH_4)_2SO_4$ particles show

354 little or no signal of $CH_3SO_3^-$ characteristic for methanesulfonate salts.

355   In principle, a combination of static and dynamic modes of operation of the TOF-

356   SIMS allows monitoring of chemical speciation of compounds within particles [*Gaspar, et al.*,

357   2004; *Laskin, Gaspar, et al.*, 2003; *Liu, et al.*, 2007]. However, these experiments are technically

358   challenging, and inherently qualitative, providing no quantitative information on the

359   concentrations of different species within particles. An alternative approach uses

360   STXM/NEXAFS analysis to study chemical bonding information of different elements for

361   individual particles. Supported by the TOF-SIMS observations, this enables the speciation of

362   different elements within particles allowing quantification of $CH_3SO_3^-/SO_4^{2-}$ ratios in

363   individual particles.

364   Figure 9(a) shows a representative STXM image (12 μm × 12 μm) recorded at 290.8

365   eV of a sample region containing two particle classes observed in our experiments. Contours

366   of the sea salt and the S-rich particles in the STXM image are marked by squares and circles,

367   respectively. Maps generated by principle component analysis (PCA) of the acquired

368   STXM/NEXAFS spectra are shown, with colors corresponding to X-ray absorbance regions

369   specific for nitrogen, carbon and sulfur. In contrast to the TOF-SIMS maps, these PCA

370   maps generated from STXM/NEXAFS analysis are indicative of the entire composition of

371   sampled particles due to the fact that transmitted intensity through the sample is measured.

372   Comparison of the PCA maps presented in Figure 9(b) and (c) shows that these particles

373   either contain carbon or nitrogen, but not both elements. This observation is consistent with

374   particles having either mixed sea salt/$CH_3SO_3^-/SO_4^{2-}$ (red) or mixed $H_2SO_4/(NH_4)_2SO_4$

375   (black) composition. The spectral contours of the N K-edge NEXAFS spectra of the mixed

376     $H_2SO_4/(NH_4)_2SO_4$ and purchased $(NH_4)_2SO_4$ are nearly identical (unpublished data), which

377   is further evidence that these small round particles are mixed $H_2SO_4/(NH_4)_2SO_4$. The low

378   carbon absorption in purchased CH_3SO_3Na and the sea salt/$CH_3SO_3^-/nss-SO_4^{2-}$ particles

16

379   made peak assignments in their spectra ambiguous, thus preventing comparisons of the C-K

380   edge NEXAFS spectra. The PCA maps presented in Figure 9(d) indicate two different types

381   of sulfur characteristic for two particle classes. The particles which contain nitrogen (black)

382   display a sulfur L-edge NEXAFS spectrum indicative of SO_4^{2-} which is consistent with these

383   particles being assigned as mixed $H_2SO_4/(NH_4)_2SO_4$. The particles which contain carbon

384   (red) display a sulfur L-edge spectrum that is intermediate of $CH_3SO_3^-$ and SO_4^{2-}. This is

385   consistent with these particles having a mixed sea salt/$CH_3SO_3^-$/SO_4^{2-} composition.

386   Furthermore, combined data sets from CCSEM/EDX and STXM/NEXAFS

387   measurements, enable quantification of the $CH_3SO_3^-/SO_4^{2-}$ ratios on an individual particle

388   basis. Elemental analysis performed using CCSEM/EDX measures the total S/Na ratio for a

389   large number of particles. Separately, STXM/NEXAFS analysis provides quantification of

390   the partitioning between $CH_3SO_3^-$ and total-SO_4^{2-} (nss and ss) on an individual particle basis.

391   Combining these two data sets, in addition to the literature reported value for ss-SO_4^{2-}/Na

392   = 0.06 [*CRC*, 1999], enables the total-SO_4^{2-} to be decoupled into nss and ss components,

393   leading to the quantitative assessment of $CH_3SO_3^-$/nss-SO_4^{2-} ratios in particles as will be

394   described below.

395   Figure 10(a) presents S L-edge NEXAFS spectra of the Na_2SO_4 and CH_3SO_3Na

396   reference particles respectively. The Na_2SO_4 spectrum displays three distinct peaks at 170.9

397   eV, 172.1 eV and 172.9 eV, in good agreement with literature data [*Hitchcock, et al.*, 1990].

398   Sulfur spectra recorded from $(NH_4)_2SO_4$ and Na_2SO_4, both of which have an oxidation state

399   of +6, were identical to one another. However, the CH_3SO_3Na spectrum is considerably

400   different, its broad contour has no resolvable peaks and the peak maximum occurs at lower

401   energy. The peak maximum of the Na_2SO_4 spectrum (or sulfate in general) appears at higher

402   energy because of its higher oxidation state (+6 for Na_2SO_4 versus +5 for CH_3SO_3Na).

403 These differences in the spectral contours of SO_4^{2-} and $CH_3SO_3^-$ are advantageous for

404 determining the partitioning between these two species in individual particles. Mixing of

405 $CH_3SO_3^-$ and SO_4^{2-} in particle spectra would lead to a broadening of the resolved peaks

406 present in SO_4^{2-} and a change in the relative intensities of the three peaks. These changes in

407 spectral contours as a function of the proportion of $CH_3SO_3^-$ and SO_4^{2-} were used to

408 quantify the amount of $CH_3SO_3^-$ and total-SO_4^{2-} present in individual particles. For

409 example, the $CH_3SO_3^-$/total-SO_4^{2-} ratio from the single particle pertinent to Figure 10(b) is

410 determined as 20:80%. The corresponding spectrum modeled for 20% $CH_3SO_3^-$ and 80%

411 total-SO_4^{2-} is shown for comparison. A good agreement between the spectral contours is

412 observed. Further details about the sulfur L-edge spectroscopy are provided in Supplement

413 B.

414   As STXM/NEXAFS is significantly more time and labor intensive than

415 CCSEM/EDX, a single CVI sample from the studied time period was selected for

416 quantitative analysis. A CVI sample was chosen due to the higher proportion of mixed sea

417 salt/$CH_3SO_3^-$/nss-SO_4^{2-} particles. Several other CVI and AOS samples from this time

418 period were surveyed using STXM/NEXAFS, and confirmed qualitative observations

419 reported for the selected sample in this publication. The STXM/NEXAFS analysis method

420 was applied to sulfur L-edge spectra recorded from ~100 individual mixed sea

421 salt/$CH_3SO_3^-$/nss-SO_4^{2-} particles to determine their $CH_3SO_3^-$/total-SO_4^{2-} ratio. In Figure

422 11 the $CH_3SO_3^-$/total-SO_4^{2-} ratio is plotted against the average particle diameter. As most

423 particles are irregular in shape, the equivalent circle diameter was calculated from the particle

424 projection area. The error bars displayed in Figure 11 represent the standard deviation in the

425 mean $CH_3SO_3^-$/total-SO_4^{2-} ratio, which is derived from the calibration plot presented in

426 Supplement B. No obvious size dependence was observed in the $CH_3SO_3^-$/total-SO_4^{2-} ratio

427   for the particles studied, which ranged from ~1 – 5 µm in diameter. Hence, the mean

428    $CH_3SO_3^-$/total-SO_4^{2-} ratio, represented by the solid black line in Figure 11 (the two dashed

429   lines are the standard deviation from the mean), yield a value of 0.52 with a standard

430   deviation of $\pm$ 0.30, assuming invariance with particle size.

431   Figure 12(a) presents the normalized distribution of the total-S/Na ratios detected in

432   over 7000 individual sea salt/$CH_3SO_3^-$/nss-SO_4^{2-} particles using the CCSEM/EDX

433   technique. The frequency of particles displaying a particular total S/Na ratio is normalized to

434   the total number of particles examined. This data is plotted for different size bins with

435   particle diameters ranging from 0.3 to > 2 µm. The size bins are set using the log(D_p) scale

436   with an even spacing of 0.2, where D_p represents particle diameter. The total S/Na ratio is

437   between 0.05 – 1 and peaks at 0.15 for particles in all size bins. This peak total S/Na value of

438   0.15 is higher than that characteristic for sea water (0.06) [*CRC*, 1999]. The higher observed

439   value can be understood by considering acid displacement reactions of NaCl/$MgCl_2$ present

440   in sea water with H_2SO_4 and CH_3SO_3H, which increase the total S present in the particles.

441   Sea salt fully reacted with H_2SO_4 would yield a total S/Na ratio of 0.59. Clearly, the range of

442   total S/Na values observed in these multi-component particles exceeds this, reaching values

443   as high as 1. Again, this higher observed value can be understood by considering reactions of

444   NaCl/$MgCl_2$ with CH_3SO_3H, which may yield a total S/Na ratio of 1.18. An enhancement in

445   the fraction of particles displaying total S/Na ratios > 0.15 is observed for smaller particles

446   that display larger surface-to-volume ratios. This observation could suggest that surface area

447   controls the uptake of gas-phase CH_3SO_3H by liquid sea salt particles. The longer average

448   atmospheric residence times of smaller particles may also increase the probability of reaction

449   resulting in $CH_3SO_3^-$ and nss-SO_4^{2-} enrichment.

450   As noted above, calculation of the $CH_3SO_3^-$/nss-SO_4^{2-} ratio relies on a combination

451   of data recorded using both STXM/NEXAFS and CCSEM/EDX. The method for

452   combining this data is presented here. For the mixed sea salt/$CH_3SO_3^-$/nss-SO_4^{2-} particles,

453   the total S/Na ratio is equal to the sum of ss-SO_4^{2-}/Na, nss-SO_4^{2-}/Na and $CH_3SO_3^-$/Na

454   ratios, as described by equation 3:

455

456
$$\frac{[\text{total-S}]}{[\text{Na}]} = \underbrace{\frac{\left[\text{ss-SO}_4^{2-}\right]}{[\text{Na}]}}_{= 0.06} + \frac{\left[\text{nss-SO}_4^{2-}\right]}{[\text{Na}]} + \frac{\left[\text{CH}_3\text{SO}_3^-\right]}{[\text{Na}]} \tag{3}$$

457

458   The ss-SO_4^{2-}/Na ratio is 0.06 [*CRC*, 1999], leaving two unknowns in this equation. The

459    $CH_3SO_3^-$/total-SO_4^{2-} ratio is determined as 0.52 ± 0.30 using the STXM/NEXAFS

460   technique. This ratio can be written as follows:

461

462
$$\frac{\left[\text{CH}_3\text{SO}_3^-\right]}{\left[\text{total-SO}_4^{2-}\right]} = \frac{\left[\text{CH}_3\text{SO}_3^-\right]/[\text{Na}]}{\left[\text{total-SO}_4^{2-}\right]/[\text{Na}]} = \frac{\left[\text{CH}_3\text{SO}_3^-\right]/[\text{Na}]}{0.06 + \left[\text{nss-SO}_4^{2-}\right]/[\text{Na}]} \tag{4}$$

463   This leaves the same two unknowns as in equation 3. These two equations can now be

464   solved to determine values for both $[CH_3SO_3^-]$/[Na] and [nss-SO_4^{2-}]/[Na].

465   This analysis method is applied to the data presented in Figure 12(a) to yield Figure

466   12(b), which displays the distribution of $CH_3SO_3^-$/nss-SO_4^{2-} in individual particles for

467   different size bins. As particle diameter increases, the distribution of $CH_3SO_3^-$/nss-SO_4^{2-}

468   shifts to higher values, *i.e.* sulfur in larger particles is mostly in the form of $CH_3SO_3^-$, while

469   sulfur content in smaller particles is dominated by the SO_4^{2-} form.

470   The peak of the distribution presented in Figure 12(b), which uses the mean

471 $CH_3SO_3^-$/total-SO_4^{2-} ratio of 0.52, yields a $CH_3SO_3^-$/nss-SO_4^{2-} partitioning ratio of 0.6.

472 Using the standard deviation in the mean CH_3SO_3Na/total-SO_4^{2-} ratio of ±0.30, the lower

473 and upper limits on the $CH_3SO_3^-$/nss-SO_4^{2-} ratio are calculated as 0.30 and 1.10. The large

474 variation in this ratio could be attributed to differences in the individual particle history, the

475 long duration over which the particles were sampled, the uncertainty associated with the

476 measurement and the assumptions associated with invariance of $CH_3SO_3^-$/SO_4^{2-} with

477 particle size.

478   Therefore, all the observations presented in this manuscript so far, can be

479 summarized as follows. Particles collected during the cloudy period between July 6th 17:00-

480 July 7th 9:00 (PST) can be divided in two major particle classes: (a) sea salt particles

481 composed of a mixture of sea salt/$CH_3SO_3^-$/SO_4^{2-} and (b) S-rich particles of mixed

482 H_2SO_4/$(NH_4)_2SO_4$ composition. Qualitatively, these observations are in agreement with the

483 schematic of the sulfur-aerosol-climate links in the MBL in Figure 1. Indeed, the presence of

484 $CH_3SO_3^-$ in sea salt particles indicates substantial formation and fast uptake of CH_3SO_3H by

485 activated droplets containing sea salt presumably resulting from the oxygen addition channel

486 in the DMS oxidation mechanism. Formation of mixed H_2SO_4/$(NH_4)_2SO_4$ particles is

487 indicative of H_2SO_4 nucleation resulting from the H abstraction channel of DMS oxidation.

488 Therefore, the quantitative assessment of partitioning between two different forms of sulfur,

489 *i.e.* $CH_3SO_3^-$ and nss-SO_4^{2-}, is important for kinetic modeling as it is an inherent indicator of

490 the pathways of DMS oxidation in the environment of the given geographic location. The

491 partitioning between these reaction products is important for climate considerations as the

492 result impacts the number and size of CCN produced in the marine atmosphere.

493   The $CH_3SO_3^-$/nss-SO_4^{2-} > 0.6 ratios in sea salt particles reported in this study are high

494   compared to previous measurements at similar latitudes. The reported ratios are similar to

495   those from polar latitudes where the temperature is lower, a factor known to enhance the

496   addition pathway leading to formation of $CH_3SO_3^-$. The results presented here are somewhat

497   comparable with model calculations which predict higher $CH_3SO_3^-$/nss-SO_4^{2-} ratios in the

498   summer for pristine marine air sampled under cold (276 K), cloudy conditions and implying

499   additional oxidation reactions of DMS with halogen radicals [*von Glasow and Crutzen*, 2004].

500   However, there is an important aspect of the presented data that contradicts modeling study

501   of *von Glasow and Crutzen* [2004]. The TOF-SIMS analysis of particle samples (see Fig. 7)

502   indicate that $CH_3SO_3^-$ is exclusively associated with sea salt particles, but not with

503     $(NH_4)_2SO_4$ particles. This finding disagrees with the modeling results that indicate significant

504   formation of $CH_3SO_3^-$ in sulfate particles as a result of their smaller size and higher surface-

505   to-volume ratio compared that typical for sea salt particles. Furthermore, despite their

506   different starting sizes, the sulfate and the sea salt particles would grow to aqueous droplets

507   that are roughly of the same size, if activated. As a result, the condensed compounds should

508   be quite similar in the different activated particles. This observed selectivity of $CH_3SO_3^-$ to

509   sea salt particles is quite puzzling and additional studies are required to understand this

510   discrepancy.

511   The discrepancy is even more intriguing given that our numerical model calculations

512   of the atmospheric chemistry occurring in the area of the field experiment suggests that

513   consideration of cloud chemistry is essentially required to explain the high $CH_3SO_3^-$/nss-

514   SO_4^{2-} and S/Na ratios reported in this study. These modeling results are presented and

515   discussed below.

516   During the cloudy period studied here, meteorological data indicate that air parcels

517   arriving to the sampling site were first swiftly transported from the open ocean area and then

518   turned southbound along the coastline of northern California (Figure 2) where it remained

519   for ~12-18 hours prior to sampling. A systematic analysis of phytoplankton pigment

520   concentrations in this area (derived from satellite based multi-annual records) indicate an

521   order of magnitude higher phytoplankton concentration in the narrow latitudinal range

522   adjacent to the shore. Specifically, within 100-200 km of the coast, typical concentrations of

523   phytoplankton of ~5 µg/l are reported, while 300-400 km offshore these decrease to ~0.5

524   µg/l [*A. C. Thomas and Strub*, 1990]. Therefore, the key factor determining the $CH_3SO_3^-$/nss-

525   SO_4^{2-} and total-S/Na ratios in sea salt particles is most likely the amount of time the air mass

526   spent in the area of high DMS emissions (high phytoplankton concentrations) which is in

527   the order of ~18 hours or less prior to sampling at Pt. Reyes.

528   A Lagrangian box-model [*Zaveri*, 1997] was used to simulate atmospheric oxidation

529   of DMS in the air mass that originated over unpolluted open ocean areas and entered the

530   region of high DMS concentration ~18 hour prior to the sampling which corresponds to ~

531   6 am local time. Two model scenarios were examined: (a) gas-phase chemistry only, and (b)

532   coupled gas- and cloud-phase chemistry. The initial conditions for model runs and a brief

533   description of the model are given in supplement C.

534   Figure 13 shows the temporal evolution of DMS, $CH_3SO_3^-$/nss-SO_4^{2-}, and total

535   S/Na for gas-chemistry only and coupled gas- and cloud-phase chemistry scenarios. A few

536   hours are required to build up the SO_2 concentration from gas-phase DMS oxidation in the

537   relatively clean air mass as it was advected along the coast over high DMS emissions region

538   for the next 12-18 hours. During this time, $CH_3SO_3^-$ is efficiently formed in particles, while

539   formation of nss-SO_4^{2-} is somewhat delayed. The gas-chemistry-only model results indicate

540   that the $CH_3SO_3^-$/nss-SO_4^{2-} ratio in sea salt particles reaches a maximum of ~0.18 during the

541   early stages of DMS oxidation (<6 hours) because formation of CH_3SO_3H proceeds more

542   rapidly early in the day when compared to H_2SO_4 formation. Later, as both OH and SO_2

543   concentrations increase, formation of H_2SO_4 begins to exceed that of CH_3SO_3H, resulting in

544   a decrease in the particulate $CH_3SO_3^-$/nss-SO_4^{2-} ratio to a quasi-steady-state value of ~0.13,

545   which is about a factor of 5 lower than the observed ratios seen in Figure 11b. Also, a

546   negligible increase in the modeled values of the total-S/Na ratio is seen even after 18 hours

547   of processing, which is at odds with the measurements for the field-collected sea salt

548   particles as seen in Figure 11a.

549   Atmospheric conditions during our field study most likely resemble the coupled gas

550   and cloud chemistry scenario. Indeed, the coupled gas- and cloud-phase model results show

551   that the $CH_3SO_3^-$/nss-SO_4^{2-} bulk ratio in sea salt particles reached a maximum of ~0.3 in ~6

552   hours and then remained fairly steady for the rest of the simulation period. This value is

553   comparable within a factor of ~2 to our measurements. Also, the total-S/Na bulk ratio is

554   predicted to increase up to ~0.09 in 12 hours, which is similar to the observed values. These

555   results therefore suggest that cloud-phase oxidation of SO_2, DMS, DMSO, MSIA, and MSA

556   played an important role under the atmospheric conditions encountered during this field

557   study.

558   We note that the purpose of these modeling calculations is to evaluate the feasibility

559   of the plausible hypothesis rather than providing detailed cross-comparison between field

560   and modeling data, which lies beyond the scope of this manuscript. With this regard, it is

561   important to note that modeled $CH_3SO_3^-$/nss-SO_4^{2-} and total-S/Na ratios is sensitive to a

562   number of parameters, which include DMS flux, temperature, sea-salt particle concentration

563   and size distribution, and photolysis rate. Additionally, halogen chemistry and nucleation

564 (new particle formation) were neglected in the present model, but may play an important

565 role. The influence of these parameters are interesting topics for more detailed modeling

566 studies where the field data provided here could be used for validation.

567

568 **5.   CONCLUSIONS AND ATMOPHERIC IMPLICATIONS**

569   This study presents the first observations of both $CH_3SO_3^-$ and SO_4^{2-} sulfur

570 compounds in marine aerosol, identified on a single particle basis. Both TOF-SIMS and

571 STXM/NEXAFS techniques indicate an external mixture consisting primarily of two

572 particle classes; mixed sea salt/$CH_3SO_3^-$/SO_4^{2-} and S-rich particles of mixed

573 H_2SO_4/$(NH_4)_2SO_4$ composition. Unambiguous, qualitative speciation of sulfur containing

574 compounds and quantitative assessment of the $CH_3SO_3^-$/nss-SO_4^{2-} ratios are facilitated

575 using combined data sets from three techniques: CCSEM/EDX – quantitative assessment of

576 elemental composition of individual particles, TOF-SIMS – qualitative molecular speciation

577 of sulfur-containing compounds in individual particles, STXM/NEXAFS – quantitative

578 assessment of different forms of sulfur within individual particles. The data provided by

579 these techniques offer a rich set of qualitative and quantitative information that is of primary

580 importance to atmospheric processes in the MBL involving sea salt and marine sulfate

581 particles.

582   For the first time, size-dependent nss-S/Na and $CH_3SO_3^-$/nss-SO_4^{2-} ratios are

583 reported for marine particles. Characteristic ratios of nss-S/Na > 0.10 are reported for sea

584 salt particles, with higher values observed for smaller particles, indicating more extensive

585 formation of sulfur-containing salts. Characteristic ratios of $CH_3SO_3^-$/nss-SO_4^{2-} > 0.60 are

586 reported for sea salt particles of all sizes, with higher values for large particles. This indicates

587   that $CH_3SO_3^-$ salts are likely the dominant form of nss-sulfur in large particles while SO_4^{2-} is

588   more common in smaller particles.

589   In the past, much attention has been given to the hygroscopic and optical properties

590   of sea salt aerosol and the corresponding mixed sea salt/sulfate particles that can be formed

591   as a result of the $DMS{\rightarrow}SO_2{\rightarrow}H_2SO_4$ reaction sequence that is assumed to dominate in the

592   mid-latitude marine boundary layer. However, our analysis of field collected sea salt particles

593   and presented in this manuscript indicate that DMS conversion to MSA can result in

594    $CH_3SO_3^-/SO_4^{2-}$ >0.6 and nss-S/Na >0.1 ratios, as were observed under specific conditions

595   of the coastal area north of San Francisco. These findings indicate that modeling of the

596   marine boundary layer (MBL) aerosols and cloud formation processes require extensive data

597   on the hygroscopic and CCN properties of mixed sea salt/$CH_3SO_3^-$/SO_4^{2-} and perhaps other

598   organo-sulfur particles. These data are fairly scarce and require future research.

599

Supplemental Information Available:

Supplement A - TOF-SIMS spectra of particles prepared from purchased standard materials.

Supplement B - Determination of $CH_3SO_3^-$/total-SO_4^{2-} ratio in individual sea salt particles

Supplement C - Description of the model and key constraints.

623   **References**

624   Allen, A. G., A. L. Dick, and B. M. Davison (1997), Sources of atmospheric
625   methanesulphonate, non-sea-salt sulphate, nitrate and related species over the
626   temperate South Pacific, *Atmospheric Environment*, *31*, 191-205.

627   Andreae, M. O., and H. Raemdonck (1983), Dimethyl Sulfide in the Surface Ocean and the
628   Marine Atmosphere - a Global View, *Science*, *221*, 744-747.

629   Andreae, T. W., M. O. Andreae, H. G. Bingemer, and C. Leck (1993), Measurements of
630   Dimethyl Sulfide and H$_2$S over the Western North-Atlantic and the Tropical
631   Atlantic, *Journal of Geophysical Research-Atmospheres*, *98*, 23389-23396.

632   Arsene, C., I. Barnes, K. H. Becker, W. F. Schneider, T. T. Wallington, N. Mihalopoulos,
633   and I. V. Patroescu-Klotz (2002), Formation of methane sulfinic acid in the gas-
634   phase OH-radical initiated oxidation of dimethyl sulfoxide, *Environmental Science and*
635   *Technology*, *36*, 5155-5163.

636   Bandy, A. R., D. L. Scott, B. W. Blomquist, S. M. Chen, and D. C. Thornton (1992), Low
637   Yields of SO$_2$ from Dimethyl Sulfide Oxidation in the Marine Boundary-Layer,
638   *Geophysical Research Letters*, *19*, 1125-1127.

639   Bandy, A. R., D. C. Thornton, F. H. Tu, B. W. Blomquist, W. Nadler, G. M. Mitchell, and
640   D. H. Lenschow (2002), Determination of the vertical flux of dimethyl sulfide by
641   eddy correlation and atmospheric pressure ionization mass spectrometry (APIMS),
642   *Journal of Geophysical Research-Atmospheres*, *107 (D24),* Art. No. 4743,
643   doi:10.1029/2002JD002472

644   Bardouki, H., M. B. da Rosa, N. Mihalopoulos, W.U. Palm, C. Zetzsch. (2002), Kinetics and
645   Mechanism of the Oxidation of Dimethylsulfoxide (DMSO) and Methanesulfinate
646   (MSI$^-$) by OH Radicals in Aqueous Medium, *Atmos. Environ., 36,* 4627–4634.

647   Barnard, W. R., M. O. Andreae, W. E. Watkins, H. Bingemer, and H. W. Georgii (1982), The
648   Flux of Dimethylsulfide from the Oceans to the Atmosphere, *Journal of Geophysical*
649   *Research-Oceans and Atmospheres*, *87*, 8787-8793.

650   Barnes, I., K. H. Becker, and N. Mihalopoulos (1994), An FTIR Product Study of the
651   Photooxidation of Dimethyl Disulfide, *Journal of Atmospheric Chemistry*, *18*, 267-289.

652   Bates, T. S., B. K. Lamb, A. Guenther, J. Dignon, and R. E. Stoiber (1992), Sulfur Emissions
653   to the Atmosphere from Natural Sources, *Journal of Atmospheric Chemistry*, *14*, 315-337.

654   Barone, S. B., A. A.Turnipseed, A. R. Ravishankara (1996), Reaction of OH with dimethyl
655   sulfide (DMS). 1. Equilibrium constant for OH+DMS reaction and the kinetics of
656   the OH•DMS+O$_2$ reaction, *J. Phys. Chem., 100 (35),* 14694-14702.

657   Berresheim, H., M. O. Andreae, G. P. Ayers, R. W. Gillett, J. T. Merrill, V. J. Davis, and W.
658   L. Chameides (1990), Airborne Measurements of Dimethylsulfide, Sulfur-Dioxide,
659   and Aerosol Ions over the Southern-Ocean South of Australia, *Journal of Atmospheric*
660   *Chemistry*, *10*, 341-370.

661 Burgermeister, S., and H. W. Georgii (1991), Distribution of Methanesulfonate, nss-Sulfate
662   and Dimethylsulfide over the Atlantic and the North-Sea, *Atmospheric Environment*
663   *Part a-General Topics*, *25*, 587-595.

664 Charlson, R. J., J. E. Lovelock, M. O. Andreae, and S. G. Warren (1987), Oceanic
665   Phytoplankton, Atmospheric Sulfur, Cloud Albedo and Climate, *Nature*, *326*, 655-
666   661.

667 Cooper, D. J., and E. S. Saltzman (1991), Measurements of Atmospheric Dimethyl Sulfide
668   and Carbon-Disulfide in the Western Atlantic Boundary-Layer, *Journal of Atmospheric*
669   *Chemistry*, *12*, 153-168.

670 Cooper, D. J., and E. S. Saltzman (1993), Measurements of Atmospheric Dimethylsulfide,
671   Hydrogen-Sulfide, and Carbon-Disulfide During Gte Cite-3, *Journal of Geophysical*
672   *Research-Atmospheres*, *98*, 23397-23409.

673 Covert, D. S., V. N. Kapustin, P. K. Quinn, and T. S. Bates (1992), New Particle Formation
674   in the Marine Boundary-Layer, *Journal of Geophysical Research-Atmospheres*, *97*, 20581-
675   20589.

676 CRC (1999), Handbook of Chemistry and Physics. A ready-reference book of chemical and
677   physics data., 80th, ed., D. R. Lide, CRC Press Inc., Boca Raton, FL.

678 Draxler, R. R., and G. D. Rolph (2003), HYSPLIT (HYbrid Single-Particle Lagrangian
679   Integrated Trajectory) Model access via NOAA ARL READY Website
680   (http://www.arl.noaa.gov/ready/hysplit4.html). NOAA Air Resources Laboratory,
681   Silver Spring, MD.

682 Finlayson-Pitts, B. J. (2003), The tropospheric chemistry of sea salt: A molecular-level view
683   of the chemistry of NaCl and NaBr, *Chemical Reviews*, *103*, 4801-4822.

684 Finlayson-Pitts, B. J., and J. C. Hemminger (2000), Physical chemistry of airborne sea salt
685   particles and their components, *Journal of Physical Chemistry A*, *104*, 11463-11477.

686 Galloway, J. N., D. L. Savoie, W. C. Keene, and J. M. Prospero (1993), The Temporal and
687   Spatial Variability of Scavenging Ratios for nss-Sulfate, Nitrate, Methanesulfonate
688   and Sodium in the Atmosphere over the North-Atlantic Ocean, *Atmospheric*
689   *Environment Part a-General Topics*, *27*, 235-250.

690 Ganor, E., H. A. Foner, H. G. Bingemer, R. Udisti, and I. Setter (2000), Biogenic sulphate
691   generation in the Mediterranean Sea and its contribution to the sulphate anomaly in
692   the aerosol over Israel and the Eastern Mediterranean, *Atmospheric Environment*, *34*,
693   3453-3462.

694 Gaspar, D. J., A. Laskin, W. Wang, S. W. Hunt, and B. J. Finlayson-Pitts (2004), TOF-SIMS
695   analysis of sea salt particles: imaging and depth profiling in the discovery of an
696   unrecognized mechanism for pH buffering, *Applied Surface Science*, *231-2*, 520-523.

697 Goldstein, J. I., D. E. Newbury, P. Echlin, D. C. Joy, C. E. Lyman, E. Lifshin, L. Sawyer,
698   and J. R. Michael (2003), *Scanning Electron Microscopy and X-ray Microanalysis*, Third
699   Edition ed., Kluwer, New York.

700 Gong, S. L. (2003), A parameterization of sea-salt aerosol source function for sub- and
701   super-micron particles, *Global Biogeochemical Cycles*, *17(4)*, Art. No. 1097,
702   doi:10.1029/2003GB002079.

703 Gong, S. L., and L. A. Barrie (2003), Simulating the impact of sea salt on global nss sulphate
704   aerosols, *Journal of Geophysical Research-Atmospheres*, *108 (D16)*, Art. No. 4516,
705   doi:10.1029/2002JD003181.

706 Gong, S. L., L. A. Barrie, and J. P. Blanchet (1997), Modeling sea-salt aerosols in the
707   atmosphere.1. Model development, *Journal of Geophysical Research-Atmospheres*, *102*,
708   3805-3818.

709 Gong, S. L., L. A. Barrie, and M. Lazare (2002), Canadian Aerosol Module (CAM): A size-
710   segregated simulation of atmospheric aerosol processes for climate and air quality
711   models - 2. Global sea-salt aerosol and its budgets, *Journal of Geophysical Research-
712   Atmospheres*, *107 (D24),* Art. No. 4779, doi:10.1029/2001JD002004.

713 Hertel, O., J. Christensen, and O. Hov (1994), Modeling of the End-Products of the
714   Chemical Decomposition of DMS in the Marine Boundary-Layer, *Atmospheric
715   Environment*, *28*, 2431-2449.

716 Hitchcock, A. P., G. Tourillon, R. Garrett, G. P. Williams, C. Mahatsekake, and C. Andrieu
717   (1990), Inner-shell excitation of gas-phase and polymer thin-film 3-alkylthiophenes
718   by electron energy loss and X-ray photoabsorption spectroscopy, *Journal of Physical
719   Chemistry*, *94*, 2327-2333.

720 Hopkins, R. J., A. V. Tivanski, B. D. Marten, and M. K. Gilles (2007), Chemical bonding and
721   structural information of black carbon reference materials and individual
722   carbonaceous atmospheric aerosols, *Journal of Aerosol Science*, *38*, 573-591.

723 Hynes, A. J., R. B. Stoker, A. J. Pounds, T. McKay, J. D. Bradshaw, J. M. Nicovich, and P.
724   H. Wine (1995), A Mechanistic Study of the Reaction of OH with Dimethyl-D(6)
725   Sulfide - Direct Observation of Adduct Formation and the Kinetics of the Adduct
726   Reaction with O_2, *Journal of Physical Chemistry*, *99*, 16967-16975.

727 Hynes, A. J., and P. H. Wine (1996), The atmospheric chemistry of dimethylsulfoxide
728   (DMSO) and mechanism of the OH+DMSO reaction, *Journal of Atmospheric
729   Chemistry*, *24*, 23-37.

730 Hynes, A. J., P. H. Wine, and D. H. Semmes (1986), Kinetics and Mechanism of OH
731   Reactions with Organic Sulfides, *Journal of Physical Chemistry*, *90*, 4148-4156.

732 Keller, M., W. Bellows, and R. Guillard (1989), Dimethylsulfide Production in Marine
733   Phytoplankton in *Biogenic Sulfur in the Environment*, edited by E. Saltzman and W.
734   Cooper, pp. 167-182, ACS, Washington, DC.

735 Kerminen, V. M., R. E. Hillamo, and A. S. Wexler (1998), Model simulations on the
736   variability of particulate MSA to non-sea-salt sulfate ratio in the marine environment,
737   *Journal of Atmospheric Chemistry*, *30*, 345-370.

738 Kettle, A.J., M.O. Andreae, D. Amouroux, T.W. Andreae, T.S. Bates, H. Berresheim, H.
739   Bingemer, R. Boniforti, M.A.J. Curran, G.R. Di Tullio, G. Helas, G.B. Jones, M.D.
740   Keller, R.P. Kiene, C. Leck, M. Levasseur, G. Malin, M. Maspero, P. Matrai, A.R.
741   McTaggart, N. Mihalopoulos, B.C. Nguyen, A. Novo, J.P. Putaud, S. Rapsomanikis,
742   G. Roberts, G. Schebeske, S. Sharma, R. Simo, R. Staubes, S. Turner and G. Uher
743   (1999), A global database of sea surface dimethylsulfide (DMS) measurements and a
744   procedure to predict sea surface DMS as a function of latitude, longitude and month,
745   *Global Biogeochem. Cycles, 13,* 399–444.

746 Kloster, S., J. Feichter, E. M. Reimer, K. D. Six, P. Stier, and P. Wetzel (2006), DMS cycle in
747   the marine ocean-atmosphere system - a global model study, *Biogeosciences*, *3*, 29-51.

748 Koga, S., and H. Tanaka (1993), Numerical Study of the Oxidation Process of
749   Dimethylsulfide in the Marine Atmosphere, *Journal of Atmospheric Chemistry*, *17*, 201-
750   228.

751 Koga, S., and H. Tanaka (1996), Simulations of seasonal variations of sulfur compounds in
752   the remote marine atmosphere, *Journal of Atmospheric Chemistry*, *23*, 163-192.

753 Koga, S., and H. Tanaka (1999), Modeling the methanesulfonate to non-sea-salt sulfate
754   molar ratio and dimethylsulfide oxidation in the atmosphere, *Journal of Geophysical
755   Research-Atmospheres*, *104*, 13735-13747.

756 Koga, S., H. Tanaka, M. Yamato, T. Yamanouchi, F. Nishio, and Y. Iwasaka (1991),
757   Methanesulfonic-Acid and Non-Sea-Salt Sulfate over Both Hemispheric Oceans,
758   *Journal of the Meteorological Society of Japan*, *69*, 1-14.

759 Kouvarakis, G., and N. Mihalopoulos (2002), Seasonal variation of dimethylsulfide in the gas
760   phase and of methanesulfonate and non-sea-salt sulfate in the aerosols phase in the
761   Eastern Mediterranean atmosphere, *Atmospheric Environment*, *36*, 929-938.

762 Laskin, A., and J. P. Cowin (2001), Automated single particle SEM/EDX analysis of
763   submicrometer particles down to 0.1 mu m, *Analytical Chemistry*, *73*, 1023-1029.

764 Laskin, A., J. P. Cowin, and M. J. Iedema (2006), Analysis of individual environmental
765   particles using modern methods of electron microscopy and X-ray microanalysis,
766   *Journal of Electron Spectroscopy and Related Phenomena*, *150*, 260-274.

767 Laskin, A., D. J. Gaspar, W. H. Wang, S. W. Hunt, J. P. Cowin, S. D. Colson, and B. J.
768   Finlayson-Pitts (2003), Reactions at interfaces as a source of sulfate formation in sea-
769   salt particles, *Science*, *301*, 340-344.

770 Laskin, A., M. J. Iedema, and J. P. Cowin (2003), Time-resolved aerosol collector for
771   CCSEM/EDX single-particle analysis, *Aerosol Science and Technology*, *37*, 246-260.

772 Lewis, E. R., and S. E. Schwartz (2004), *Sea Salt Aerosol Production: Mechanisms, Methods,
773   Measurements and Models - A Critical Review*, 413 pp., AGU, Washington, DC.

774 Li, S. M., and L. A. Barrie (1993), Biogenic Sulfur Aerosol in the Arctic Troposphere.1.
775   Contributions to Total Sulfate, *Journal of Geophysical Research-Atmospheres*, *98*, 20613-
776   20622.

777 Li, S. M., L. A. Barrie, and A. Sirois (1993), Biogenic Sulfur Aerosol in the Arctic
778   Troposphere.2. Trends and Seasonal-Variations, *Journal of Geophysical Research-
779   Atmospheres*, *98*, 20623-20631.

780 Li, S. M., L. A. Barrie, R. W. Talbot, R. C. Harriss, C. I. Davidson, and J. L. Jaffrezo (1993),
781   Seasonal and Geographic Variations of Methanesulfonic-Acid in the Arctic
782   Troposphere, *Atmospheric Environment Part a-General Topics*, *27*, 3011-3024.

783 Li, S. M., L. A. Barrie, and D. Toom (1996), Seasonal variations of methanesulfonate, non-
784   sea-salt sulfate, and sulfur dioxide at three sites in Canada, *Journal of Geophysical
785   Research-Atmospheres*, *101*, 4165-4173.

786 Liss, P. S., and L. Merlivat (1986), Air-sea gass exchange rates, in *The Role of Air-Sea Exchange*
787   *in Geochemical Cycling*, edited by P. Buat-Menard, pp. 113-127, Reidel, Dordrecht.

788 Liu, Y., Z. Yang, Y. Desyaterik, P. L. Gassman, H. Wang, and A. Laskin (2007), Probing
789   Hygroscopic Properties of Atmospheric Particles Using Complementary Methods of
790   Micro FTIR Spectroscopy and Micro Analyses, *Environmental Science and Technology*,
791   submitted.

792 Lucas, D. D., and R. G. Prinn (2002), Mechanistic studies of dimethylsulfide oxidation
793   products using an observationally constrained model, *Journal of Geophysical Research-*
794   *Atmospheres*, *107(D14),* Art. No. 4201, doi:10.1029/2001JD000843.

795 Lucas, D. D., and R. G. Prinn (2003), Tropospheric distributions of sulfuric acid-water
796   vapor aerosol nucleation rates from dimethylsulfide oxidation, *Geophysical Research*
797   *Letters*, *30 (22),* Art. No. 2136, doi:10.1029/2003GL018370.

798 Lucas, D. D., and R. G. Prinn (2005a), Parametric sensitivity and uncertainty analysis of
799   dimethylsulfide oxidation in the clear-sky remote marine boundary layer, *Atmospheric*
800   *Chemistry and Physics*, *5*, 1505-1525.

801 Lucas, D. D., and R. G. Prinn (2005b), Sensitivies of gas-phase dimethylsulfide oxidation
802   products to the assumed mechanisms in a chemical transport model, *Journal of*
803   *Geophysical Research-Atmospheres*, *110*, Art. No. D21312, doi:10.1029/2004JD005386

804 Maria, S. F., L. M. Russell, M. K. Gilles, and S. C. B. Myneni (2004), Organic aerosol growth
805   mechanisms and their climate-forcing implications, *Science*, *306*, 1921-1924.

806 MASE (2005), Marine Stratus Experiment (MASE) 2005, URL:
807   http://www.asp.bnl.gov/MASE.html.

808 Mihalopoulos, N., B. C. Nguyen, C. Boissard, J. M. Campin, J. P. Putaud, S. Belviso, I.
809   Barnes, and K. H. Becker (1992), Field-Study of Dimethylsulfide Oxidation in the
810   Boundary-Layer - Variations of Dimethylsulfide, Methanesulfonic-Acid, Sulfur-
811   Dioxide, Non-Seasalt Sulfate and Aitken Nuclei at a Coastal Site, *Journal of*
812   *Atmospheric Chemistry*, *14*, 459-477.

813 Murphy, D. M., J. R. Anderson, P. K. Quinn, L. M. McInnes, F. J. Brechtel, S. M.
814   Kreidenweis, A. M. Middlebrook, M. Posfai, D. S. Thomson, and P. R. Buseck
815   (1998), Influence of sea-salt on aerosol radiative properties in the Southern Ocean
816   marine boundary layer, *Nature*, *392*, 62-65.

817 Ogren, J. A., J. Heintzenberg, and R. J. Charlson (1985), In-situ Sampling of Clouds with a
818   Droplet to Aerosol Converter, *Geophysical Research Letters*, *12*, 121-124.

819 Quinn, P. K., D. S. Covert, T. S. Bates, V. N. Kapustin, D. C. Ramseybell, and L. M.
820   McInnes (1993), Dimethylsulfide Cloud Condensation Nuclei Climate System -
821   Relevant Size-Resolved Measurements of the Chemical and Physical-Properties of
822   Atmospheric Aerosol-Particles, *Journal of Geophysical Research-Atmospheres*, *98*, 10411-
823   10427.

824 Ravishankara, A.R., Y. Rudich, R. Talukdar, S.B. Barone, (1997) Oxidation of atmospheric
825   reduced sulphur compounds: Perspective from laboratory studies, *Philosophical Trans.*
826   *Royal Soc. London. Series B -Biological Sci, 352 (1350)*, 171-181.

827 Russell, L. M., S. F. Maria, and S. C. B. Myneni (2002), Mapping organic coatings on
828   atmospheric particles, *Geophysical Research Letters*, *29*, 1779.

829 Saltzman, E. S., D. L. Savoie, J. M. Prospero, and R. G. Zika (1985), Atmospheric
830   Methanesulfonic-Acid and Non-Sea-Salt Sulfate at Fanning and American Samoa,
831   *Geophysical Research Letters*, *12*, 437-440.

832 Saltzman, E. S., D. L. Savoie, J. M. Prospero, and R. G. Zika (1986), Methanesulfonic-Acid
833   and Non-Sea-Salt Sulfate in Pacific Air - Regional and Seasonal-Variations, *Journal of*
834   *Atmospheric Chemistry*, *4*, 227-240.

835 Saltzman, E. S., D. L. Savoie, R. G. Zika, and J. M. Prospero (1983), Methane Sulfonic-Acid
836   in the Marine Atmosphere, *Journal of Geophysical Research-Oceans and Atmospheres*, *88*,
837   897-902.

838 Sciare, J., E. Baboukas, M. Kanakidou, U. Krischke, S. Belviso, H. Bardouki, and N.
839   Mihalopoulos (2000), Spatial and temporal variability of atmospheric sulfur-
840   containing gases and particles during the Albatross campaign, *Journal of Geophysical*
841   *Research-Atmospheres*, *105*, 14433-14448.

842 Shaw, G. E. (1983), Bio-Controlled Thermostasis Involving the Sulfur Cycle, *Climatic Change*,
843   *5*, 297-303.

844 Sievering, H., J. Boatman, J. Galloway, W. Keene, Y. Kim, M. Luria, and J. Ray (1991),
845   Heterogeneous Sulfur Conversion in Sea-Salt Aerosol-Particles - the Role of Aerosol
846   Water-Content and Size Distribution, *Atmospheric Environment Part a-General Topics*, *25*,
847   1479-1487.

848 Sievering, H., J. Cainey, M. Harvey, J. McGregor, S. Nichol, and P. Quinn (2004), Aerosol
849   non-sea-salt sulfate in the remote marine boundary layer under clear-sky and normal
850   cloudiness conditions: Ocean-derived biogenic alkalinity enhances sea-salt sulfate
851   production by ozone oxidation, *Journal of Geophysical Research-Atmospheres*, *109,* Art.
852   No. D19317, doi:10.1029/2003JD004315.

853 Spicer, C. W., D. V. Kenny, E. Chapman, K. M. Busness, and C. M. Berkowitz (1996),
854   Observations of dimethyl sulfide over the western North Atlantic Ocean using an
855   airborne tandem mass spectrometer, *Journal of Geophysical Research-Atmospheres*, *101*,
856   29137-29147.

857 Spiro, P. A., D. J. Jacob, and J. A. Logan (1992), Global Inventory of Sulfur Emissions with
858   1' × 1' Resolution, *Journal of Geophysical Research-Atmospheres*, *97*, 6023-6036.

859 Stickel, R. E., J. M. Nicovich, S. Wang, Z. Zhao, and P. H. Wine (1992), Kinetic and
860   Mechanistic Study of the Reaction of Atomic Chlorine with Dimethyl Sulfide, *Journal*
861   *of Physical Chemistry*, *96*, 9875-9883.

862 Strub, P. T., C. James, A. C. Thomas, and M. R. Abbott (1990), Seasonal and Nonseasonal
863   Variability of Satellite-Derived Surface Pigment Concentration in the California
864   Current, *Journal of Geophysical Research-Oceans*, *95*, 11501-11530.

865 Thomas, A., and P. T. Strub (2001), Cross-shelf phytoplankton pigment variability in the
866   California Current, *Continental Shelf Research*, *21*, 1157-1190.

867 Thomas, A. C., and P. T. Strub (1990), Seasonal and Interannual Variability of Pigment
868   Concentrations across a California Current Frontal Zone, *Journal of Geophysical*
869   *Research-Oceans*, *95*, 13023-13042.

870 Thompson, A. M., and O. C. Zafiriou (1983), Air-sea fluxes of transient atmospheric species,
871   *Journal of Geophysical Research - Atmospheres*, *88*, 6696-6708.

872 Tivanski, A. V., R. J. Hopkins, T. Tyliszczak, and M. K. Gilles (2007), Oxygenated interface
873   on biomass burn tar balls determined by single particle scanning transmission X-ray
874   microscopy, *Journal of Physical Chemistry A*, *111*, 5448-5458.

875 Turnipseed, A. A., S. B. Barone, A. R. Ravishankara (1996), Reaction of OH with dimethyl
876   sulfide .2. Products and mechanisms, *J. Phys. Chem., 100(35),* 14703-14713

877 Urbanski, S. P., R. E. Stickel, and P. H. Wine (1998), Mechanistic and kinetic study of the
878   gas-phase reaction of hydroxyl radical with dimethyl sulfoxide, *Journal of Physical*
879   *Chemistry A*, *102*, 10522-10529.

880 von Glasow, R., and P. J. Crutzen (2004), Model study of multiphase DMS oxidation with a
881   focus on halogens, *Atmospheric Chemistry and Physics*, *4*, 589-608.

882 von Glasow, R., R. Sander, A. Bott, and P. J. Crutzen (2002a), Modeling halogen chemistry
883   in the marine boundary layer - 1. Cloud-free MBL, *Journal of Geophysical Research-*
884   *Atmospheres*, *107 (D17)*, Art. No. 4341, doi:10.1029/2001JD000942

885 von Glasow, R., R. Sander, A. Bott, and P. J. Crutzen (2002b), Modeling halogen chemistry
886   in the marine boundary layer - 2. Interactions with sulfur and the cloud-covered
887   MBL, *Journal of Geophysical Research-Atmospheres*, *107 (D17),* Art. No. 4323,
888   doi:10.1029/2001JD000943.

889 Wong, C. S., S. E. Wong, W. A. Richardson, G. E. Smith, M. D. Arychuk, and J. S. Page
890   (2005), Temporal and spatial distribution of dimethylsulfide in the subarctic
891   northeast Pacific Ocean: a high-nutrient-low-chlorophyll region, *Tellus Series B-*
892   *Chemical and Physical Meteorology*, *57*, 317-331.

893 Wylie, D. J., and S. J. deMora (1996), Atmospheric dimethylsulfide and sulfur species in
894   aerosol and rainwater at a coastal site in New Zealand, *Journal of Geophysical Research-*
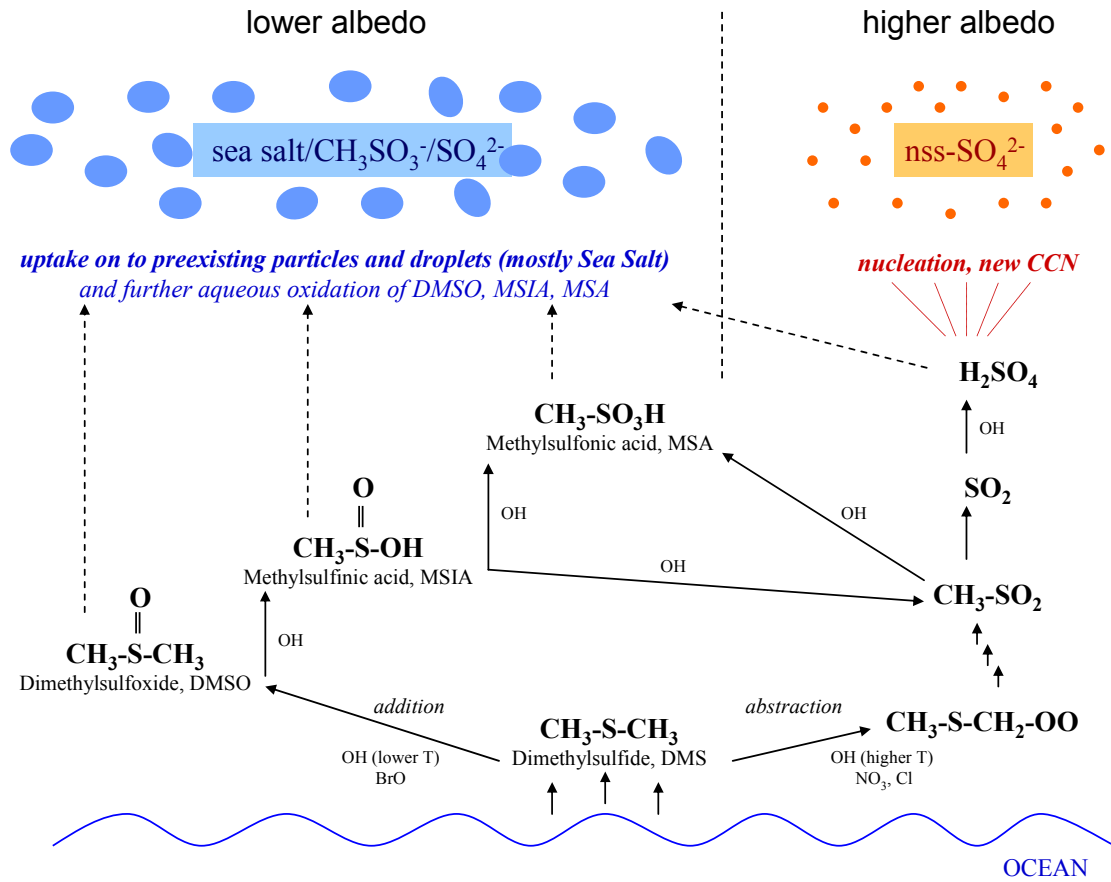895   *Atmospheres*, *101*, 21041-21049.

896 Yin, F. D., D. Grosjean, R. C. Flagan, and J. H. Seinfeld (1990), Photooxidation of Dimethyl
897   Sulfide and Dimethyl Disulfide. 2. Mechanism Evaluation, *Journal of Atmospheric*
898   *Chemistry*, *11*, 365-399.

899 Yin, F. D., D. Grosjean, and J. H. Seinfeld (1986), Analysis of Atmospheric Photooxidation
900   Mechanisms for Organosulfur Compounds, *Journal of Geophysical Research-Atmospheres*,
901   *91*, 14417-14438.

902 Yin, F. D., D. Grosjean, and J. H. Seinfeld (1990), Photooxidation of Dimethyl Sulfide and
903   Dimethyl Disulfide. 1. Mechanism Development, *Journal of Atmospheric Chemistry*, *11*,
904   309-364.

905 Zaveri, R. A. (1997), Development and Evaluation of a Comprehensive Tropospheric
906   Chemistry Model for Regional and Global Applications, Ph.D. thesis, 250 pp,
907   Virginia Polytechnic Institute and State University, Blacksburg, VA.

908 Zaveri, R. A., R. C. Easter, J. D. Fast, and L. K. Peters (2007), Model for Simulating Aerosol
909   Interactions and Chemistry (MOSAIC), *Journal of Geophysical Research - Atmospheres*,
910   submitted.

911 Zaveri, R. A., R. C. Easter, and L. K. Peters (2005), A computationally efficient
912   Multicomponent Equilibrium Solver for Aerosols (MESA), *Journal of Geophysical*
913   *Research - Atmospheres*, *110*, Art. No. D24203, doi:10.1029/2004JD005618.

914 Zaveri, R. A., R. C. Easter, and A. S. Wexler (2005), A new method for multicomponent
915   activity coefficients of electrolytes in aqueous atmospheric aerosols, *Journal of*
916   *Geophysical Research - Atmospheres*, *110*, Art. No. D02201, doi:10.1029/2004JD004681.

917 Zaveri, R. A., and L. K. Peters (1999), A new lumped structure photochemical mechanism
918   for large-scale applications, *Journal of Geophysical Research - Atmospheres*, *104*, 30387-
919   30415.

920 Zemmelink, H. J., W. W. C. Gieskes, W. Klaassen, H. W. de Groot, H. J. W. de Baar, J. W.
921   H. Dacey, E. J. Hintsa, and W. R. McGillis (2002), Simultaneous use of relaxed eddy
922   accumulation and gradient flux techniques for the measurement of sea-to-air
923   exchange of dimethyl sulphide, *Atmospheric Environment*, *36*, 5709-5717.

924 Zhao, Z., R. E. Stickel, and P. H. Wine (1996), Branching ratios for methyl elimination in the
925   reactions of OD radicals and Cl atoms with CH_3SCH_3, *Chemical Physics Letters*, *251*,
926   59-66.

927 Zhu, L., A. Nenes, P. H. Wine, and J. M. Nicovich (2006), Effects of aqueous organosulfur
928   chemistry on particulate methanesulfonate to non-sea salt sulfate ratios in the marine
929   atmosphere, *Journal of Geophysical Research-Atmospheres*, *111,* Art. No. D05316,
930   doi:10.1029/2005JD006326.

931 Zhu, L., J. M. Nicovich, and P. H. Wine (2003), Temperature-dependent kinetics studies of
932   aqueous phase reactions of hydroxyl radicals with dimethylsulfoxide,
933   dimethylsulfone, and methanesulfonate, *Aquatic Sciences*, *65*, 425-435.

934

935

lower albedo   higher albedo

sea salt/CH$_3$SO$_3^-$/SO$_4^{2-}$ nss-SO$_4^{2-}$

uptake on to preexisting particles and droplets (mostly Sea Salt)
and further aqueous oxidation of DMSO, MSIA, MSA

nucleation, new CCN

H$_2$SO$_4$

OH

CH$_3$-SO$_3$H
Methylsulfonic acid, MSA

SO$_2$

OH   OH   OH

O
||
CH$_3$-S-OH
Methylsulfinic acid, MSIA

OH   **CH$_3$-SO$_2$**

OH

O
||
CH$_3$-S-CH$_3$
Dimethylsulfoxide, DMSO

addition   *abstraction*   **CH$_3$-S-CH$_2$-OO**

OH (lower T)   **CH$_3$-S-CH$_3$**   OH (higher T)
BrO   Dimethylsulfide, DMS   NO$_3$, Cl

OCEAN

936

937   **Figure 1** Schematic diagram of sulfur-aerosol-climate links in the MBL (adopted from *von*
938   *Glasow and Crutzen*, 2004).

939

940

941
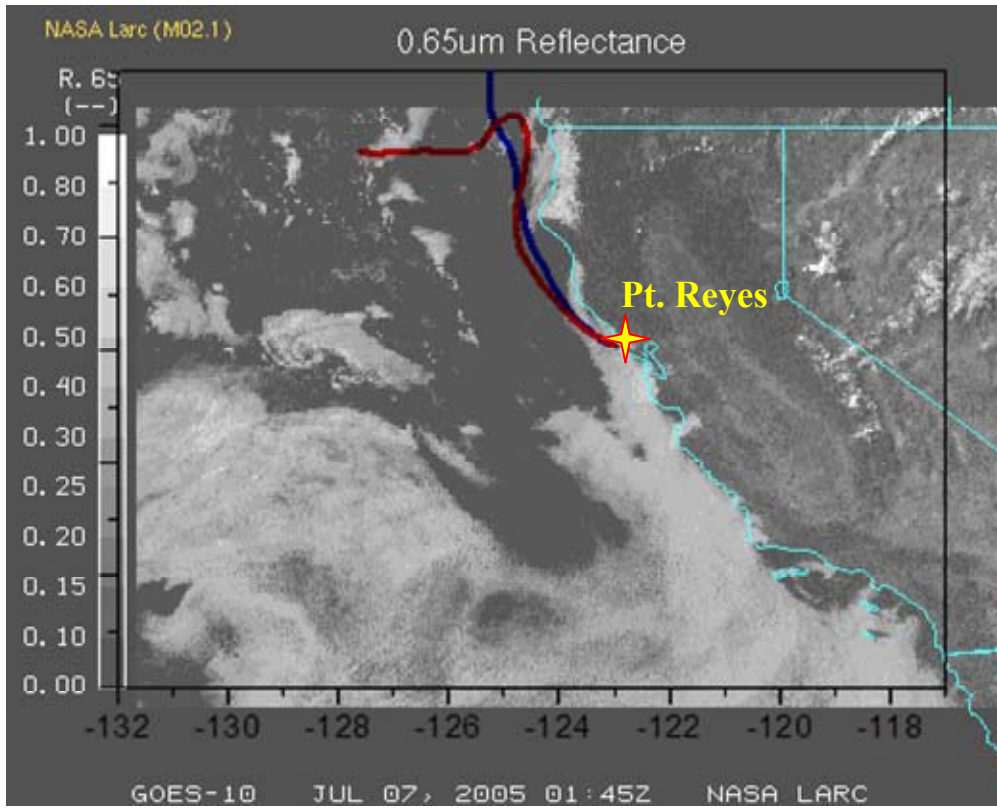
Figure 2 GOES-10 satellite image (0.65 micron cloud reflectivity at 4 km resolution) of the
California coast, at July 6, 17:45 PST (July 7, 1:45 UTC), showing extensive coastal stratus
typical of this region. Superimposed on this image are 48 hour HYSPLIT backtrajectories
starting at 10 m AGL on July 6, 21:00 PST (red) and July 7, 09:00 PST (blue)

946

947
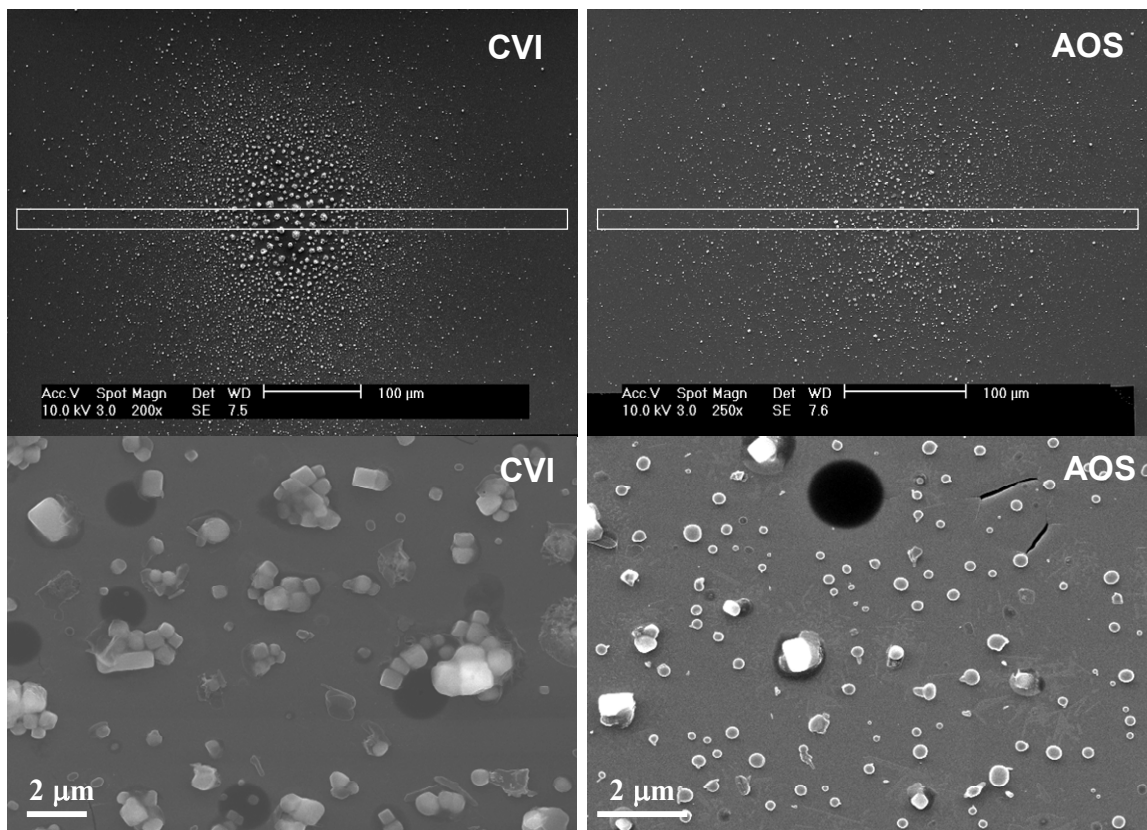
949
950
951 **Figure 3** SEM images of two samples collected from the CVI and AOS sampling lines
952 during the cloudy period on July 7, 2005. The upper images are the entire samples and
953 illustrate the spatial inhomogeneity of the deposition spot. Rectangles indicate the regions
954 inspected by CCSEM/EDX analysis. The lower images are magnified fields of view,
955 showing representative particles from the central areas of the samples. Sea salt particles are
956 larger, irregularly shaped supermicron particles with NaCl cubic crystal cores. Ammonium
957 sulfate particles are spherical submicron particles.
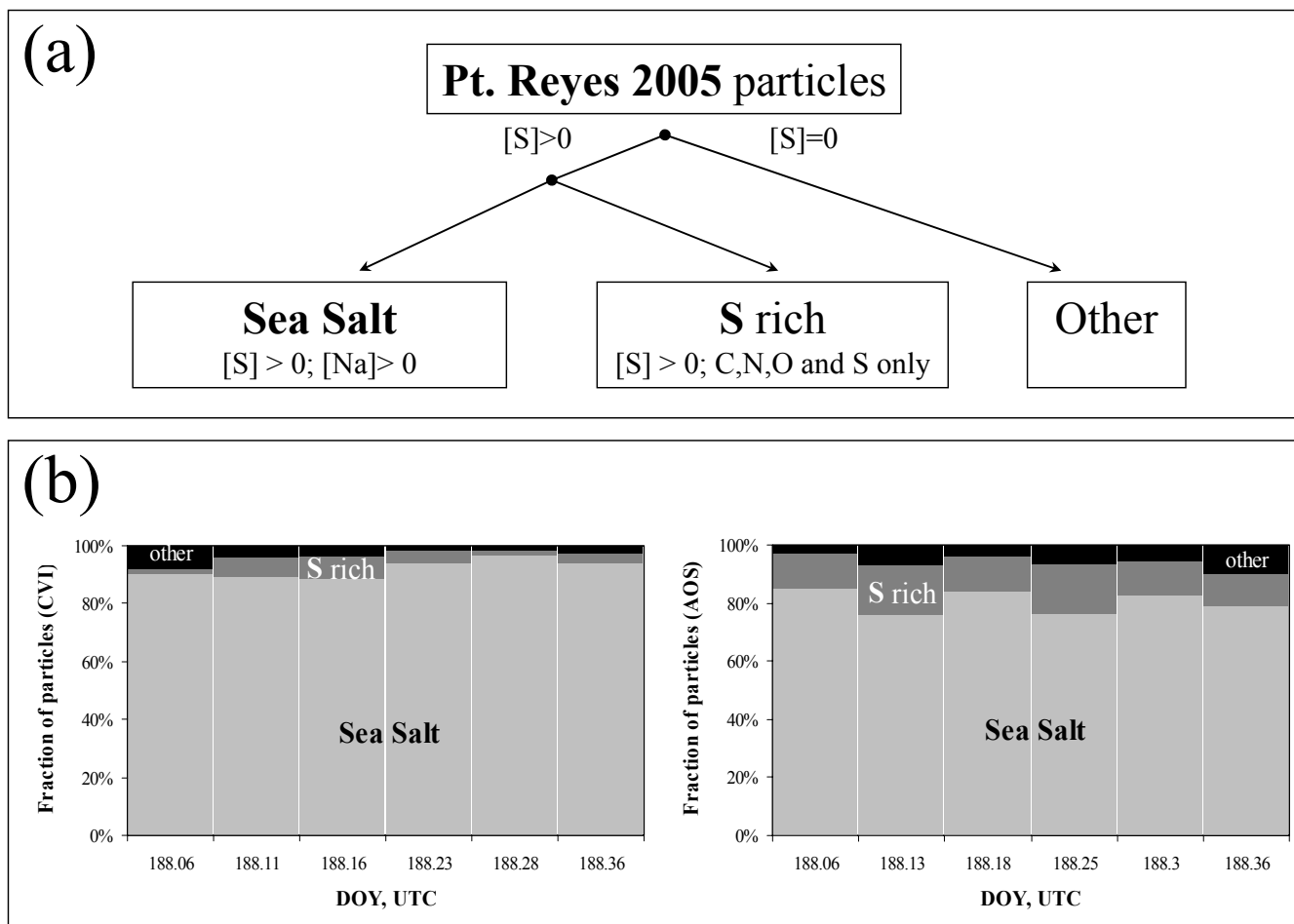
Figure 4 (a) Classification scheme applied to the samples collected during the cloudy period on the night of July 7, 2005 (Point Reyes 2005). (b) Stacked column chart diagram of particle-classes present in the CVI (left panel) and the AOS (right panel) samples.
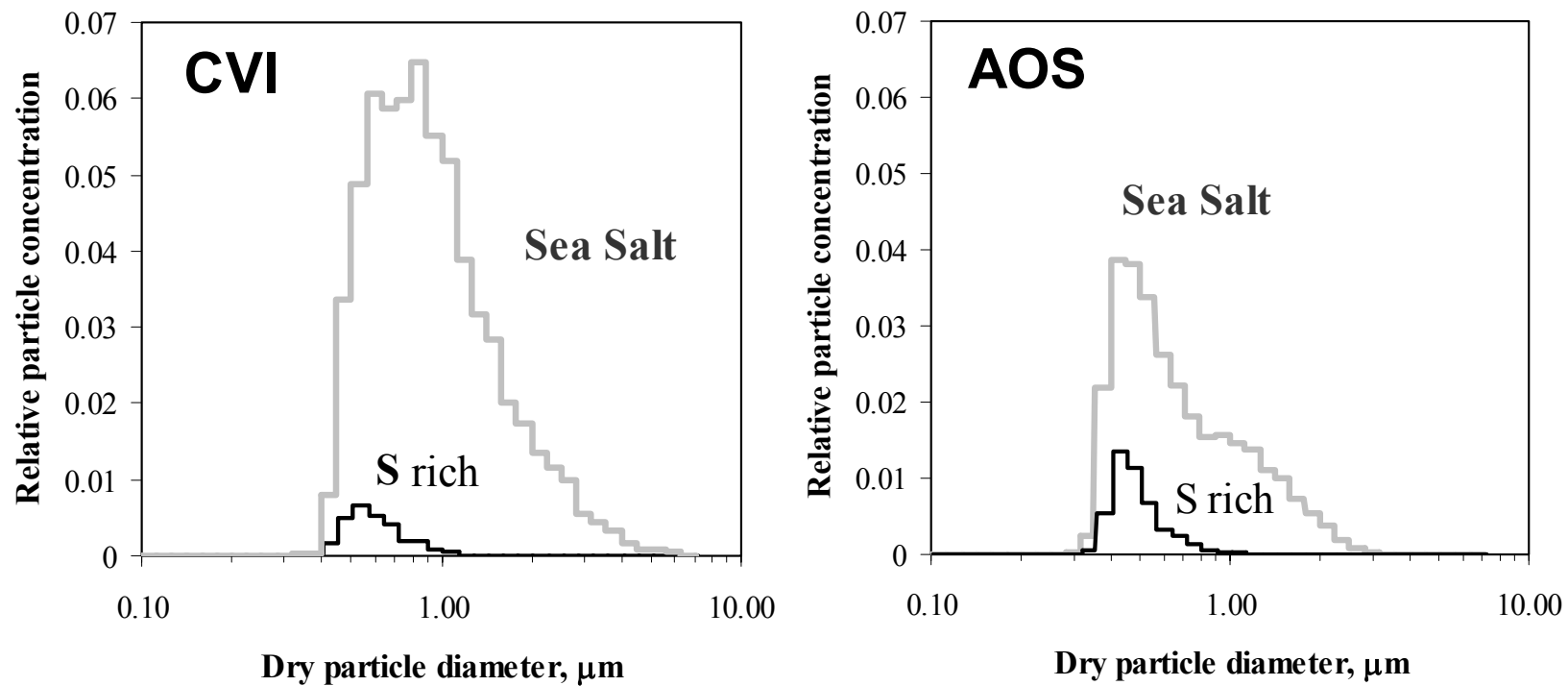
Figure 5 Number distributions of sea salt and S-rich particles in CVI (left panel) and AOS (right panel) samples measured by the CCSEM/EDX analysis. For comparison purposes, all distributions are normalized to the total number of analyzed particles.
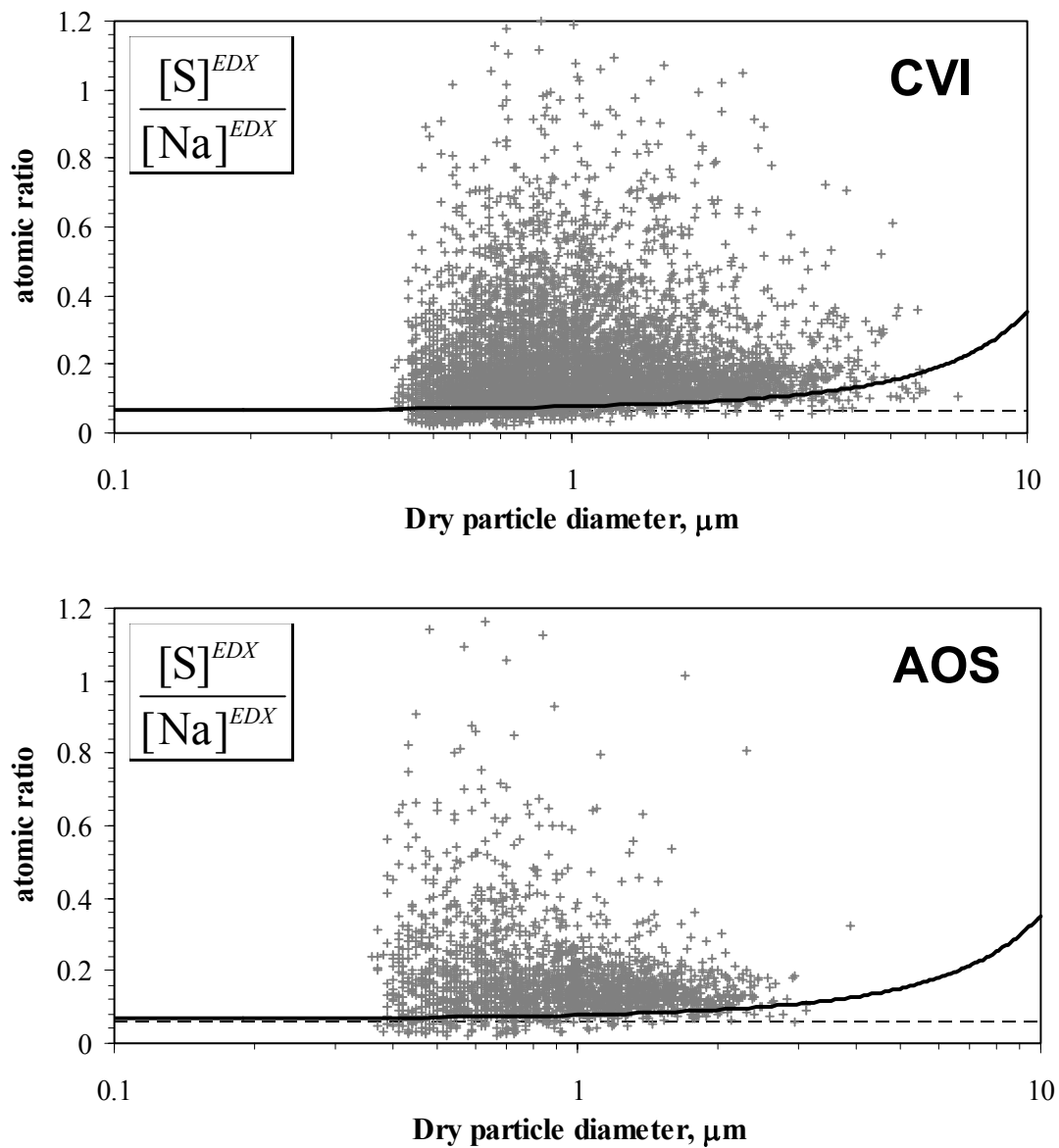
Figure 6 Elemental ratios of S/Na measured by CCSEM/EDX analysis in sea salt particles found in the CVI (upper panel) and the AOS (lower panel) samples. The dashed lines indicate the ratio of 0.06 nominal to sea water. The solid lines indicate expected experimental deviation from the nominal line from sensitivity effects that impact results of EDX particle analysis. See text for further discussion.
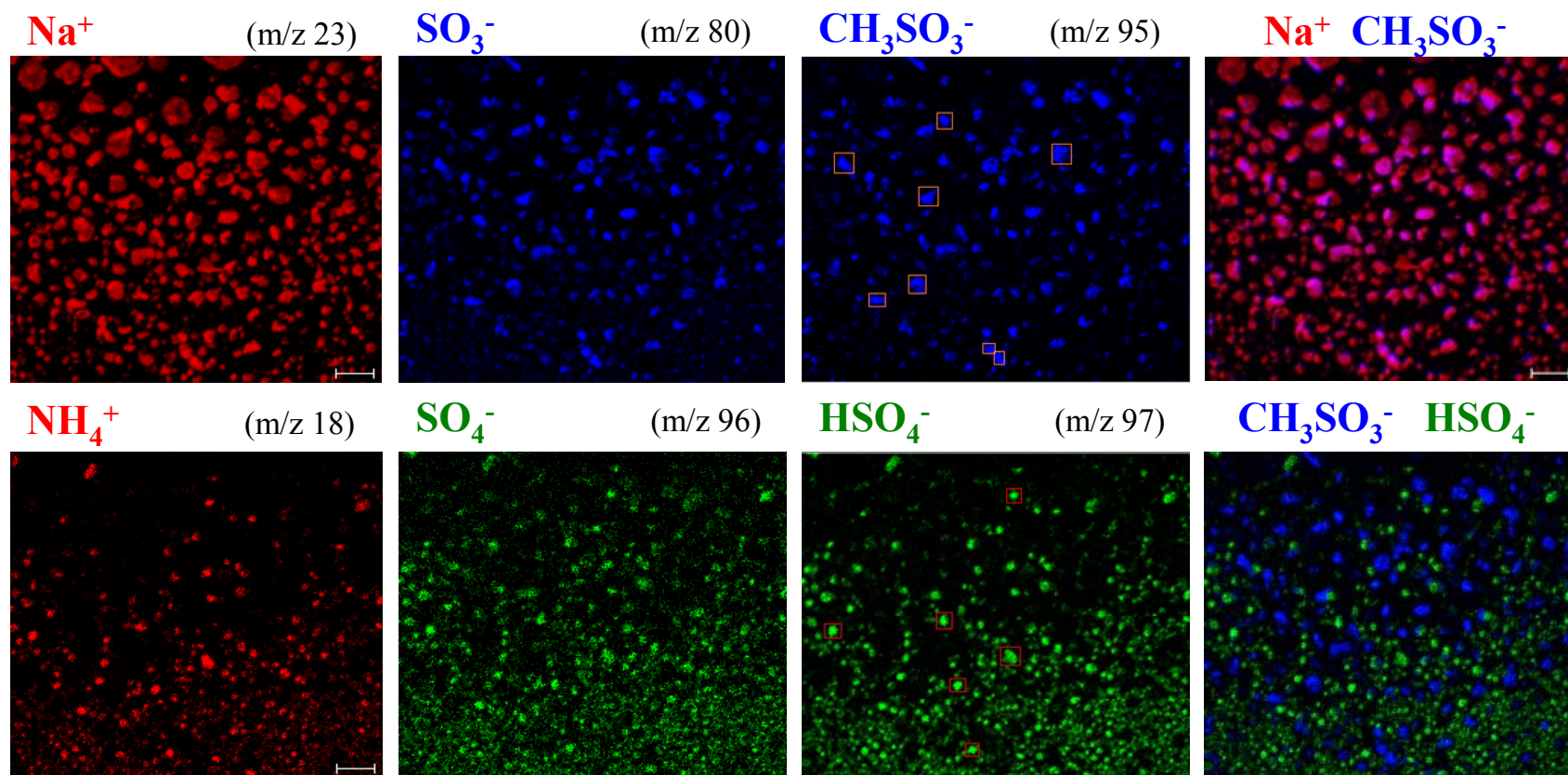
Figure 7 TOF-SIMS maps of typical samples collected from the CVI line. Upper three left images are maps produced for characteristic ions of sodium (Na^+) and methanesulfonate (SO_3^-, $CH_3SO_3^-$). The upper right image shows overlaid maps of the Na^+ and $CH_3SO_3^-$ ions. Their close overlap indicates formation of methanesulfonate in sea salt particles. The lower three left images are maps produced for characteristic ions of ammonia (NH_4^+) and sulfate (SO_4^-, HSO_4^-) originating from $H_2SO_4/(NH_4)_2SO_4$ particles. The lower right image shows overlaid maps of $CH_3SO_3^-$ and HSO_4^- ions and indicates external mixing of sea salt and ammonium sulfate particles. Maps are 100 μm × 100 μm. See text for additional details.
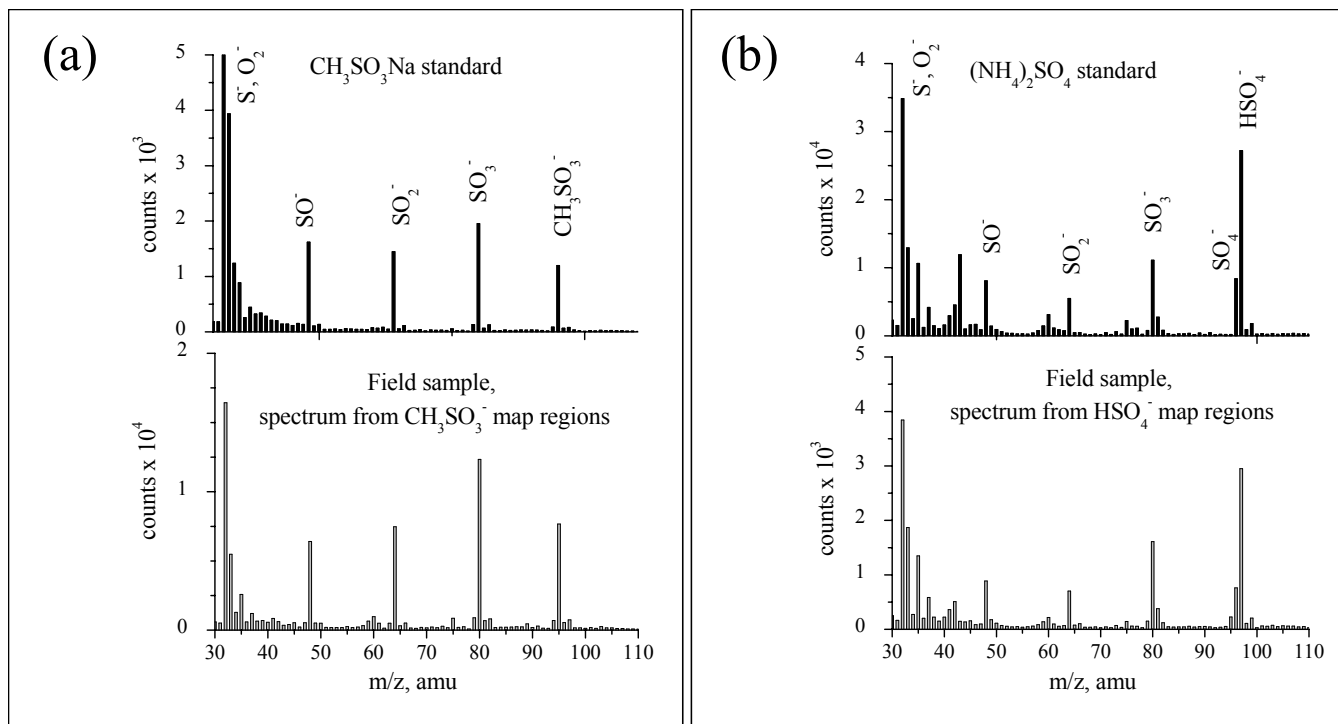
Figure 8 (a) TOF-SIMS spectrum characteristic of sea salt particles (see upper panel of Fig. 7) shown with the reference spectrum obtained from laboratory prepared CH_3SO_3Na particles. (b) TOF-SIMS spectrum characteristic of ammonium sulfate particles (see bottom panel of Fig. 7) plotted along with the reference spectrum obtained from laboratory prepared $(NH_4)_2SO_4$ particles.
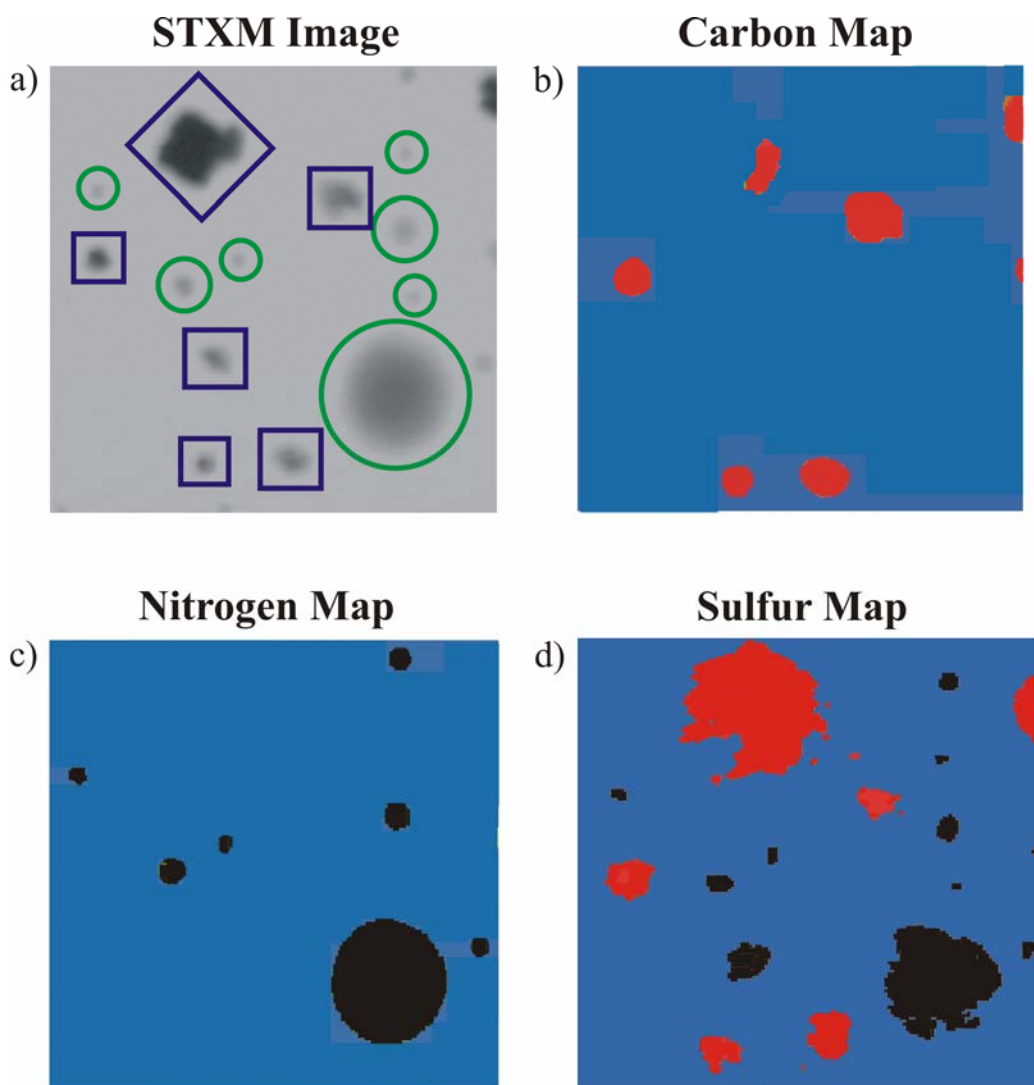
Figure 9 (a) STXM image (12 μm × 12 μm) of externally mixed sea salt/$CH_3SO_3^-$/SO_4^{2-} (marked by squares) and H_2SO_4/$(NH_4)_2SO_4$ (marked by circles) particles, b) C K-edge STXM/NEXAFS map of sea salt/$CH_3SO_3^-$/SO_4^{2-} particles, c) N K-edge STXM/NEXAFS map of H_2SO_4/$(NH_4)_2SO_4$ particles, d) S L-edge STXM/NEXAFS map of sea salt/$CH_3SO_3^-$/SO_4^{2-} particles (red) and H_2SO_4/$(NH_4)_2SO_4$ particles (black).
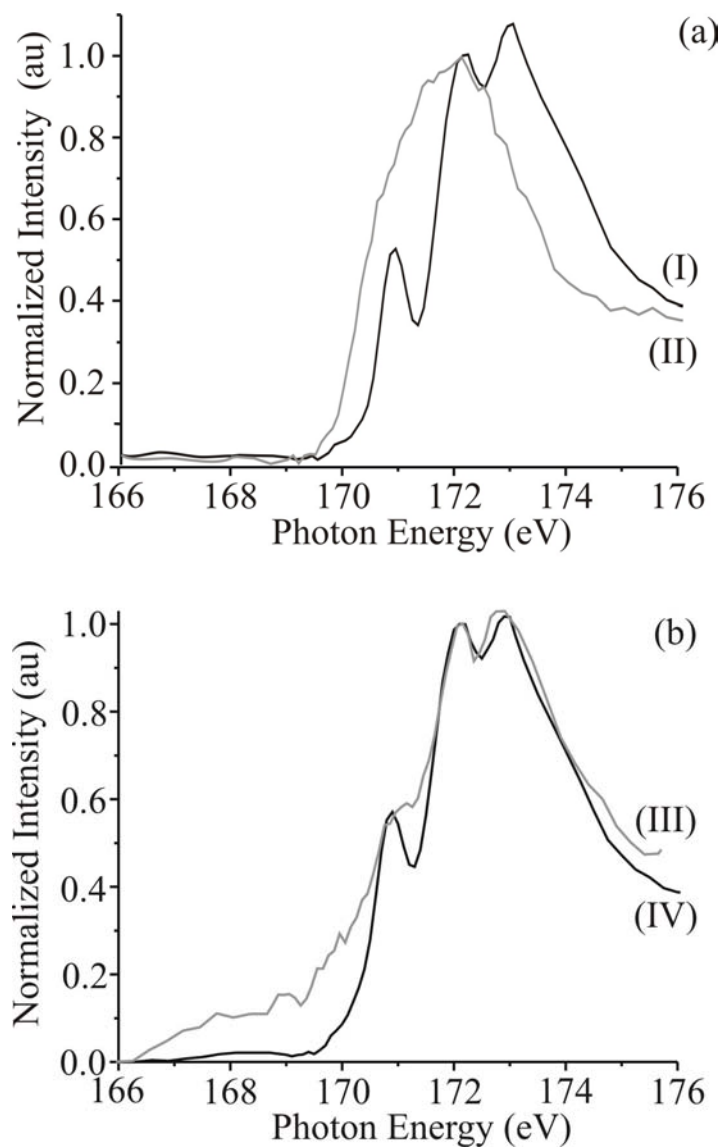
Figure 10 (a) Sulfur L-edge NEXAFS spectra recorded from reference particles of (I) Na_2SO_4 and (II) CH_3SO_3Na. (b) Sulfur L-edge NEXAFS spectrum recorded from a mixed (III) sea salt/$CH_3SO_3^-$/nss-SO_4^{2-} particle collected at Point Reyes National Seashore, (IV) modeled spectrum for 20:80 proportion of CH_3SO_3Na/Na_2SO_4 particle.
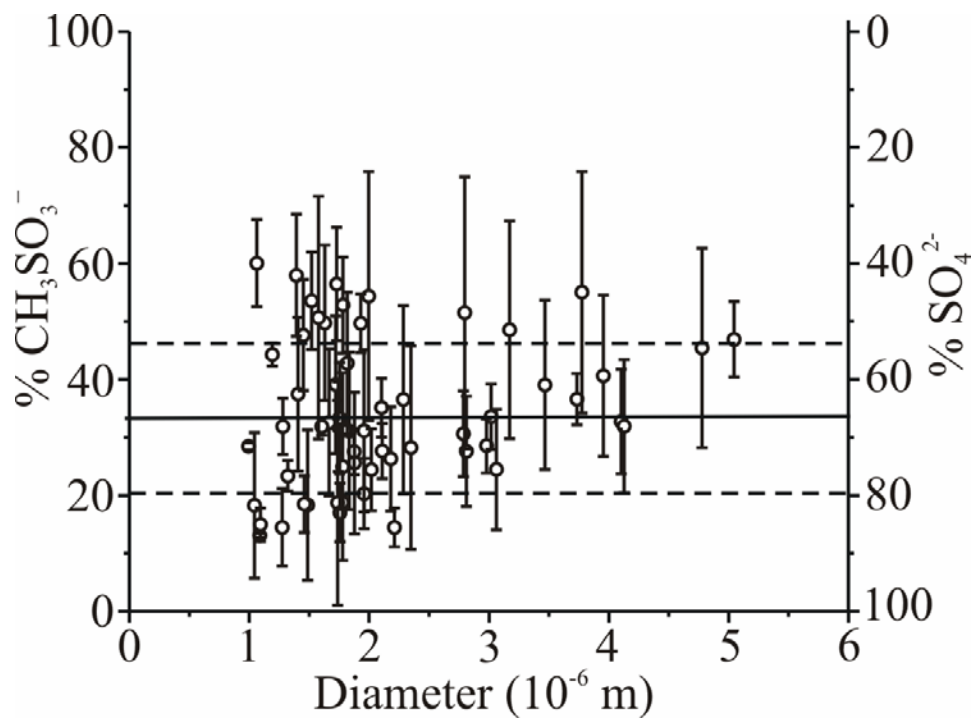
45

Figure 11 – Invariance in chemical composition with projected particle diameter. The solid black line indicates the mean value of the $CH_3SO_3^-/SO_4^{2-}$ ratio and the dashed lines represent one standard deviation from the mean.
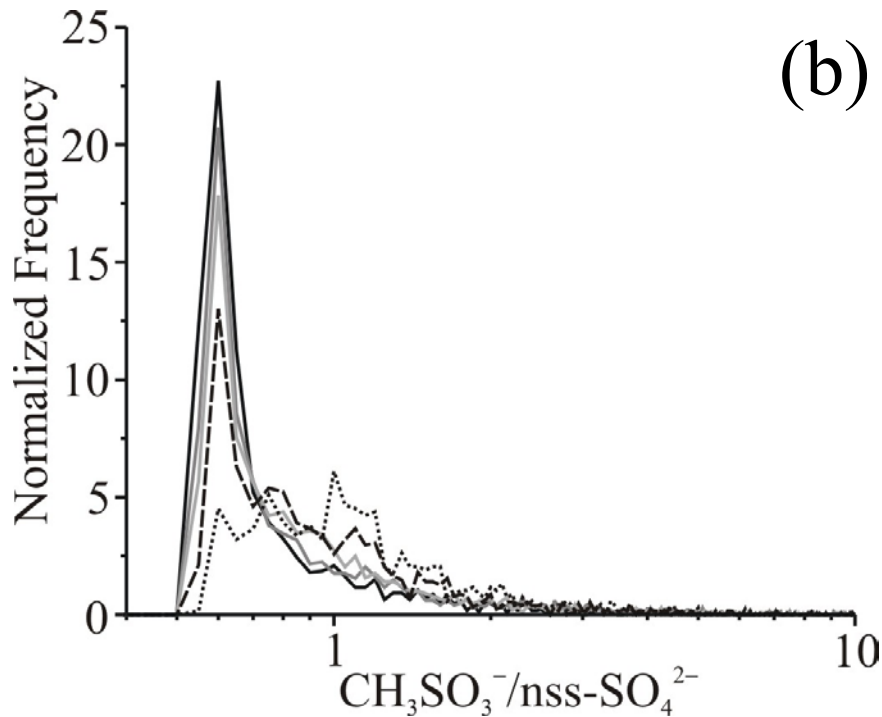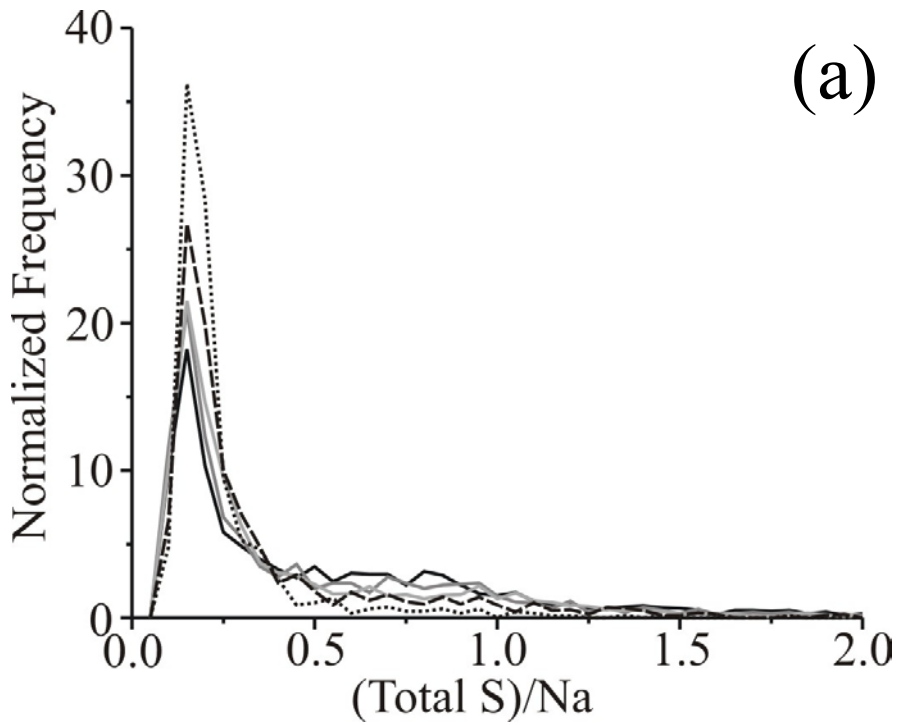
Figure 12 – Distribution of (a) total sulfur to sodium ratio and (b) $CH_3SO_3^-$ to nss-SO_4^{2-} ratio present in particles with diameter in the range $0.31 - 0.5$, $0.5 - 0.79$, $0.79 - 1.26$, $1.26 - 2$ and > 2 μm (black, dark grey, light grey, dashed and dotted lines, respectively).
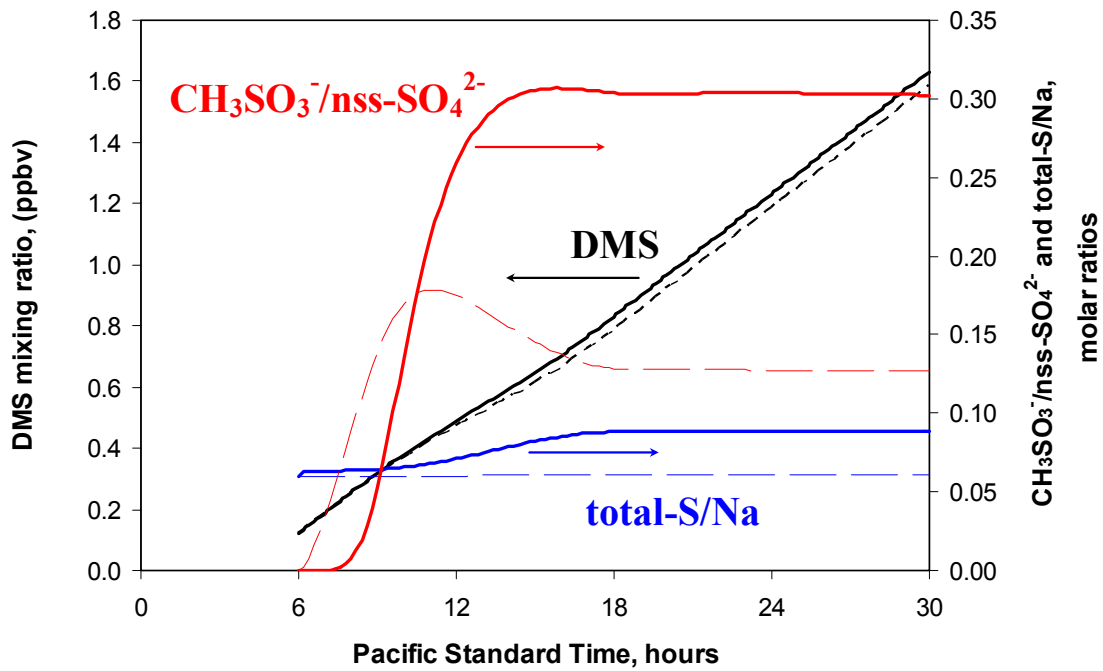
Figure 13 Temporal evolution of $[CH_3SO_3^-]/[nss\text{-}SO_4^{2-}]$ and $[total\text{-}S]/[Na]$ ratios in sea salt particles calculated using "gas-phase chemistry only" (dashed lines) and "gas and cloud chemistry" scenarios (solid lines). The model calculations are initiated at 6 am assuming $E_{DMS} = 20$ $\mu mol \cdot m^{-2} \cdot d^{-1}$, emission rates of DMS. Temporal evolution of DMS mixing ratio is also shown.